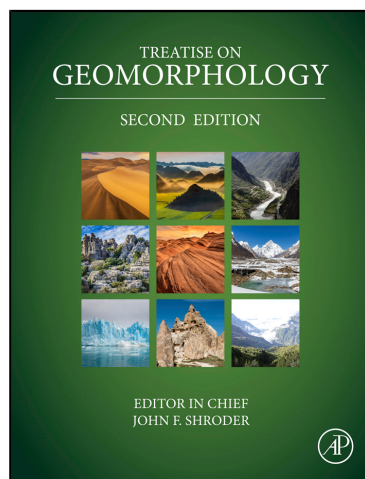


Provided for non-commercial research and educational use.
Not for reproduction, distribution or commercial use.

This article was originally published in Treatise on Geomorphology, 2nd edition, published by Elsevier, and the attached copy is provided by Elsevier for the author's benefit and for the benefit of the author's institution, for non-commercial research and educational use including without limitation use in instruction at your institution, sending it to specific colleagues who you know, and providing a copy to your institution's administrator.



All other uses, reproduction and distribution, including without limitation commercial reprints, selling or licensing copies or access, or posting on open internet sites, your personal or institution's website or repository, are prohibited. For exceptions, permission may be sought for such use through Elsevier's permissions site at:

<https://www.elsevier.com/about/our-business/policies/copyright/permissions>

From Kioka, A., Strasser, M., 2022. Oceanic Trenches. In: Shroder, J.J.F. (Ed.), Treatise on Geomorphology, vol. 8. Elsevier, Academic Press, pp. 882–900.
<https://dx.doi.org/10.1016/B978-0-12-818234-5.00167-X>.
ISBN: 9780128182345

Copyright © 2022 Elsevier Inc unless otherwise stated. All rights reserved.
Academic Press

8.32 Oceanic Trenches

Arata Kioka^a and Michael Strasser^b, ^aKyushu University, Fukuoka, Japan; and ^bUniversity of Innsbruck, Innsbruck, Austria

© 2022 Elsevier Inc. All rights reserved.

8.32.1	Introduction	882
8.32.2	History of the study of oceanic trenches and what they are	882
8.32.3	Where, how deep and how long are oceanic trenches?	886
8.32.4	Hadal trenches: The deepest places on the Earth's surface	889
8.32.5	What controls the depth of seafloor at an oceanic trench?	891
8.32.6	Isolated depositional basins at the trench axis floor	893
8.32.7	Conclusion	895
Acknowledgments		898
References		898

8.32.1 Introduction

Our home planet Earth is unique in the Solar System in that it has a vast amount of liquid water as oceans. From a geomorphological viewpoint, the Earth features a bimodal distribution of hypsography, as Mars does, while hypsographies of Venus and Earth's moon are unimodal (Fig. 1). The peaks of elevation on the Earth occur at about –4300 m and +20 m with the deepest water depth of –10,952 m in the 15-arc-second resolution digital elevation model (DEM) GEBCO 2020 Grid (GEBCO Bathymetric Compilation Group, 2020). The bimodal hypsography on the Earth can be explained by the presence of the oceans and the dichotomy between the densities of continental (granite) and oceanic (basalt) crust, a consequence of plate tectonic processes. The explanation on Mars, however, may be quite different (Smith et al., 2001). On Mars, the 200 m resolution MGS MOLA – MEX HRSC Blended DEM version 2 (Ferguson et al., 2018) shows a broader elevation range between –8530 m + 21,230 m with peaks at about –3900 m and +1500 m. A well-known deep place on the Martian surface is Valles Marineris (Golombek and Phillips, 2010), running east-west just below the equator of Mars (Fig. 2). The Valles Marineris is ~7 km deep and more than 4000 km long but may be a trough system rather than a steep trench when compared with the long but narrower width of V-shaped structured oceanic trenches on the Earth (Fig. 2). Such large V-shape structured trenches are only found on Earth in the Solar System, representing the large-scale manifestations of plate tectonics. Moreover, oceanic trenches represent the deepest places on the Earth's surface. The intrinsic curiosity of humankind to explore extremes has thus advanced exploring and understanding oceanic trenches better, in addition to the development of future political and economic opportunities.

Oceanic trenches are long and narrow depressions on the deep-sea floor, generally manifested by underthrusting oceanic lithosphere and they are developed seaward of island arcs in plate subduction zones. They are deeper than any valley found on land. Oceanic trenches are globally distributed and are now well recognized; however, they were not specifically addressed in the first edition of the *Treatise on Geomorphology*. A difference between our geomorphological understandings of the highest mountains and deepest seafloors remains as the difference between "light and shade." Oceanic trenches are geomorphologically least explored on the Earth's surface and are even less explored than Earth's Moon and Mars because of difficulties in surveying such deep depths and the profound inaccessibility and technological capacity associated with its sheer distance from the sea surface. Nevertheless, the decision to include a new chapter in the second edition of the *Treatise on Geomorphology* on the oceanic trenches is due to the recent technological advances in acquiring bathymetric data with better quality even at such deep-water depths, that have emerged in the last couple of decades. Furthermore, oceanic trenches were responsible for generating tremendous tsunamis in the 2004 Indian Ocean earthquake (Lay et al., 2005) and the 2011 Tohoku-oki earthquake (Fujii et al., 2011) which left devastating impacts on coastal communities and even the global economy. Most importantly, the scale and role of oceanic trenches indicate that they are the most significant geomorphologic features of our planet. This chapter is intended to present global and local geomorphological features of oceanic trenches worldwide on various spatial scales. This chapter provides brief reviews on (1) the history of the study of oceanic trenches and basic properties of the oceanic trenches named in the gazetteer at the International Hydrographic Organization Data Centre for Digital Bathymetry (IHO DCDB); (2) our understanding of what controls the depth of the respective oceanic trench; and (3) recent understanding in the presence of small trench-fill depositional basins along the trench axis.

8.32.2 History of the study of oceanic trenches and what they are

The presence of oceanic trenches was not clearly recognized until the 1910s. The quest to answer the question "What lies at the depths of the ocean?" has been made since 1521 when the Portuguese explorer Ferdinand Magellan first attempted to measure the depths of the Pacific Ocean. Magellan tried to measure the depth by using a sounding line – lowering a 730 m long cannonball-weighted line which did not hit the sea bottom. He realized that the area of the Pacific he measured is very deep.

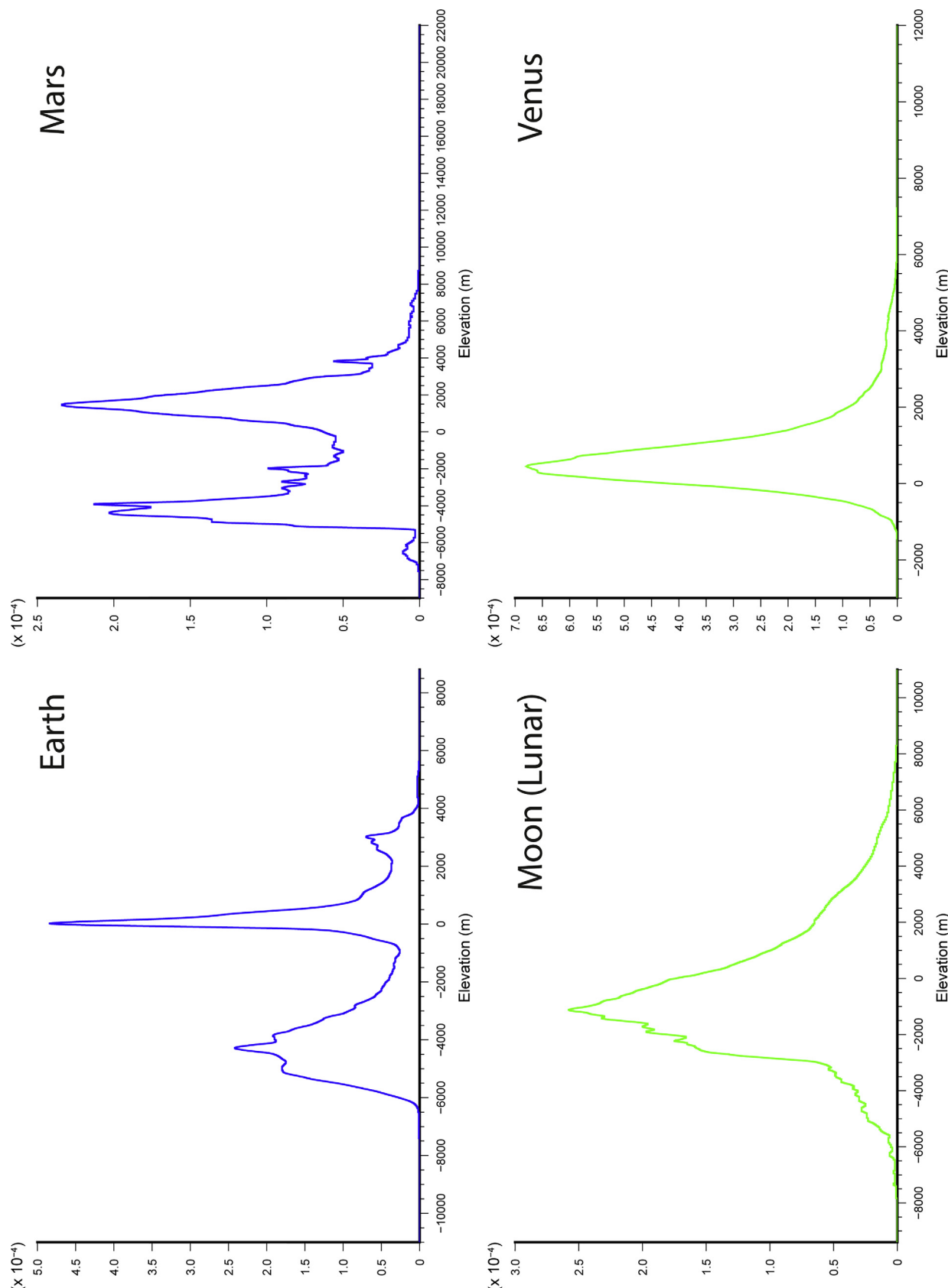


Fig. 1 Hypsometric curves of Earth, Mars, Moon (Lunar) and Venus, computed by Kernel distribution using an Epanechnikov kernel. While Lunar and Venus represent unimodal hypsography (green line), Earth and Mars are rather characterized by bimodal distributions of their hypsography (blue line). The data of DEMs for plotting the figures are from 15-arc-second resolution GEBCO 2020 Grid (GEBCO Bathymetric Compilation Group, 2020), 200 m resolution MGS MOLA – MEX HRSC Blended DEM version 2 (Ferguson et al., 2018), 118 m resolution LRO LOLA DEM version 1 (LOLA Science Team, 2014) and 4641 m resolution Magellan Global Topography version 2 (Magellan Team, 1997) for Earth, Mars, Moon and Venus, respectively. The elevation is from a gravity field solution GMM-2B for Mars and the reference radii for Moon and Venus.

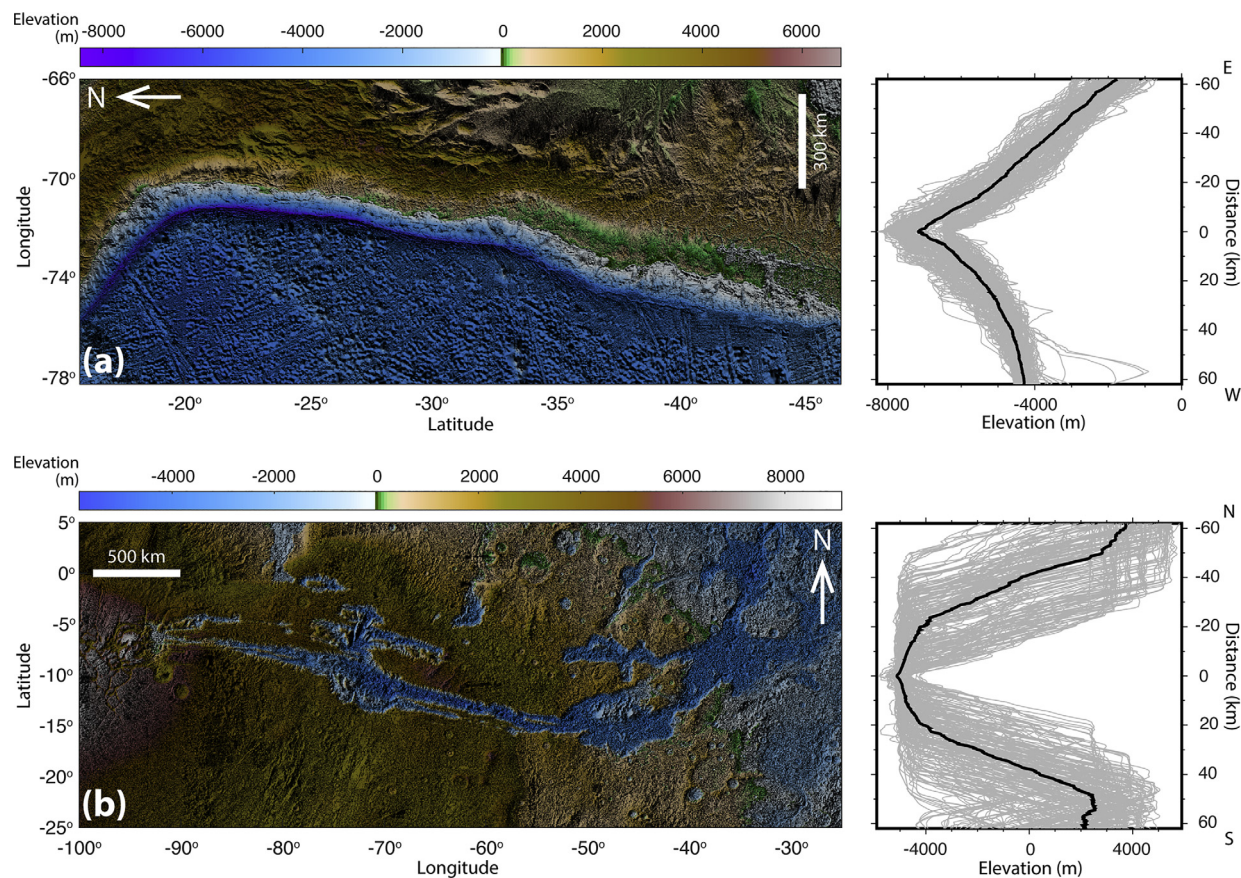


Fig. 2 Map and cross-section elevation profile of (A) typical oceanic trench on the Earth (Peru-Chile Trench, ~4000 km long) and (B) Martian “trough” Valles Marineris (~4000 km long). The cross-section elevation profile at the distance from the deepest point (trench axis) of the Peru-Chile Trench was extracted at an interval of 0.05° along latitude between 22°S and 32°S. The cross-section profile at the distance from the deepest point of the Valles Marineris was extracted at an interval of 0.05° longitude between 67°W and 57°W. The DEM data for the Peru-Chile Trench and Valles Marineris are from GEBCO 2020 Grid (GEBCO Bathymetric Compilation Group, 2020) and MGS MOLA – MEX HRSC Blended DEM version 2 (Ferguson et al., 2018), respectively.

Although many Europeans embarked on sailing around the globe, there was not much progress in exploring deep water depths in the 1600s partly because many people feared the ocean and believed in “ancient sea monsters.” The first deep sounding expedition sailed in 1773 with Lord Mulgrave’s expedition to the Arctic Ocean which recorded a depth of 680 fathoms (1250 m). In 1818, the Scottish polar explorer Sir John Ross recorded a depth of 1050 fathoms (1920 m) and collected a sediment sample in Baffin Bay, Greenland. During the expeditions of HMS *Erebus* and HMS *Terror* to the Arctic Ocean in 1839–1843, the British polar explorer Sir James Clark Ross measured water depths with a 3600 fathom (6580 m) long wire that was marked every 100 fathoms (Jamieson, 2015). The early stage of deep-sea exploration was thus centered on the surveys in the Arctic Ocean where oceanic trenches are now known to be absent. In the middle of the 19th century, a British biologist, Edward Forbes, claimed that animal life could not exist at depths greater than 550 m (Forbes, 1844). The pursuit of life deeper than 550 m and the human curiosity whether life exists in the deep oceans accelerated the progress of deep-sea exploration. In 1850, within a decade after Forbes’ statement was published, a Norwegian theologian and biologist Michael Sars sailed out to a dredging expedition in the Lofoten archipelago, Norway, and anchored around 450–500 fathoms (820–910 m) and documented the presence of a number of taxa (Hjort, 1910). In 1874, the USS *Tuscarora* expedition used a piano-wire sounding system to record a depth of 4665 fathoms (8530 m) in the Kuril-Kamchatka Trench, originally named the Tuscarora Deep (Dierssen and Theberge, 2016). In March 1875, the expedition of HMS *Challenger*, led by a British oceanographer, John Murray, and a Scottish marine zoologist, Charles Wyville Thompson, sounded the Marianas Trench using the same technique adopted during the 1839–1843 expeditions and the Challenger’s crew unexpectedly recorded 4474 fathoms (8184 m) at the point near the site thereafter called Challenger Deep (Thomson and Murray, 1895). The crews first could not believe it and sounded twice to ensure the accuracy of the sounding. These were the first measurements that unveiled the presence of ultra-deep areas, and since then, many efforts and numerous cruises have been made to determine the deepest depth of the oceans. In 1877, just 2 years after the discovery of these deepest spots, a German cartographer August Heinrich Petermann published the first bathymetric chart representing the Pacific Ocean that delineates “Challenger Tief” (Challenger Deep) and “Tuscarora Tief” (Tuscarora Deep). In the light of several expeditions to the western Pacific after the Challenger

Expedition, a German geographer Otto Krümmel published the first stand-alone map of the Mariana Trench (Krümmel, 1907). Many scientists in the late 19th and the early 20th century yet believed that deepest depths were located in other trenches in the Pacific, not in the Mariana Trench (Gardner et al., 2014). This was partly because several surveys recorded very deep water depths in the Kermadec Trench, Philippine Trench and Izu-Ogasawara (Izu-Bonin) Trench in the 1890s and 1900s using piano-wire and audio-frequency sounding methods (Jamieson, 2015). In the 1920s, a Dutch geoscientist, Felix Andries Vening Meinesz, equipped his unique gravimeter on board a submarine and discovered elongated zones of negative gravity anomalies along the Indonesian and Caribbean island arcs (Vening Meinesz, 1932). This discovery allowed him to anticipate the downwelling of the Solid Earth which was later referred to as "Tectogene" by an American geophysicist David Tressel Griggs (Griggs, 1939). Later, on 23 January 1960, the first human visit to the Challenger Deep, by Jacques Piccard and Don Walsh, was successfully made by the manned bathyscaphe (human-occupied vehicle) "Trieste" and reached a water depth of 10,913 m (Piccard and Dietz, 1961); 26 years after a spherical deep-sea submersible "bathysphere" had reached a water depth of 923 m in 1934.

The nature of these deeps was better understood in the western Pacific Ocean during World War II due to improvements and increases in bathymetric measurements using single-beam echosounders. In the late 1970s, narrow-beam multibeam echosounders became generally available for sea floor mapping (Mayer, 2006; Wölf et al., 2019). In contrast to the earlier single-beam echosounders, the multibeam echosounder system has the advantage of covering broader track with many soundings with smaller footprints. The vast improvements in multibeam echosounder system and navigation technology in the 21st century provided the impetus to revisit Earth's deepest depth, including measurement of the exact water depth of the deepest place at Challenger Deep in the Mariana Trench (Fujioka et al., 2002; Taira et al., 2005; Nakanishi and Hashimoto, 2011; Gardner et al., 2014). However, the percentage of the entire seafloor constrained by measured data or pre-prepared grids containing interpolated values is still less than 20% (Mayer et al., 2018), implying that the deep-sea features have not yet been well imaged. Moreover, measuring deeper oceanic trenches requires a larger footprint of the multibeam echosounder acquisition which reduces the horizontal resolution and results in larger uncertainty at the deep depths. These facts remain big challenges for marine geomorphology in deep water (Lecours et al., 2016) that is far behind terrestrial geomorphology.

Having said that, oceanic trenches are now clearly recognized to be the longest and largest narrow depression landforms on the Earth's surface, generally manifested by underthrusting oceanic lithosphere and developed on the seaward of island arcs in the plate subduction zones (Fig. 3; Fryer and Hussong, 1981). They are aligned into a set of convex arc shapes with remarkable continuity and depth, representing geometrically small circle arcs whose curvature relates to the subduction dip and rate. The shape of oceanic trench evolves at the equilibrium between slab pull forces and the viscous resistance of the mantle, resulting in an invariable convex shape (Frank, 1968; Tovish and Gerald, 1978; Morra et al., 2006). The cumulative length of present-day convergent plate margins is ~61,900 km (Bird, 2003; Matthews et al., 2016) almost equal to that of mid-ocean ridges (Stern, 2002). Oceanic trenches are generally 50–100 km in width and form an asymmetric V-shape depression with the steepest surface slope of up to ~10° on the landward slope (Clift and Vannucchi, 2004). Oceanic trenches are now well known to be characterized with a large negative free-air gravity anomaly, as a result of the displacement of high-density crustal materials by low-density sediments and the overlying seawater column (Talwani et al., 1959; Bassett and Watts, 2015). The material that enters oceanic trenches affects the net rate of continental growth through accretion bypassing the overriding plate wedge and underplating processes sink as residue to the core-mantle

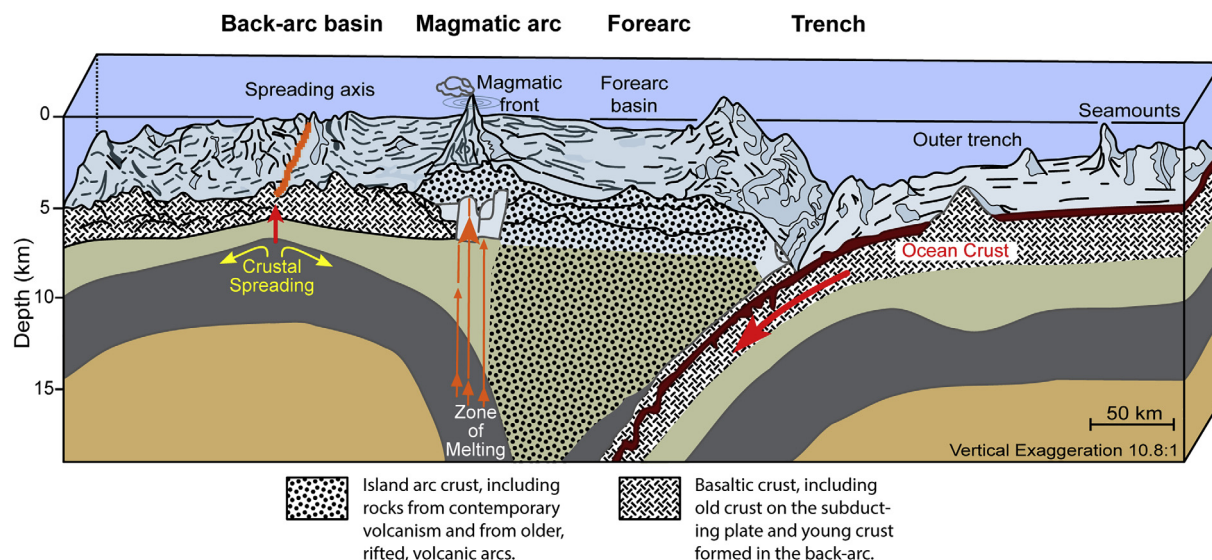


Fig. 3 Schematic illustration of oceanic trench. Modified from Fryer P and Hussong DM (1981) Seafloor spreading in the Mariana trough: Results of Leg 60 drill site selection surveys, in: Hussong DM and Uyeda S (Eds.), *Initial Reports of the Deep Sea Drilling Project, 60*. U.S. Government Printing Office. 45–55, doi:10.2973/dsdp.proc.60.103.1982.

boundary (von Huene and Scholl, 1991). Oceanic trenches are thus one of the most important surface features for understanding the evolutionary processes and dynamics of the whole earth.

Oceanic trenches were often not well distinguished from oceanic troughs. According to the International Hydrographic Organization (IHO) in 2008, a trench and a trough were defined respectively as "a long narrow, characteristically very steep and asymmetrical depression of the sea floor, with relatively steep sides" and "a long depression of the sea floor characteristically flat bottomed and steep sided and normally shallower than a TRENCH" (IHO, 2008). With the help of better imaging of deep bathymetric features, trenches were differentiated from troughs according to the deep V-shape depression feature of trenches in contrast to the relatively flat and shallow floors of troughs. Unlike oceanic trenches, oceanic troughs originate through a wide variety of mechanisms including glacial erosion and tectonic processes. Trenches are currently defined as "a long, deep, asymmetrical depression with relatively steep sides, that is associated with subduction" (IHO, 2019). This chapter focuses on oceanic trenches as defined in the gazetteer at the IHO Data Centre for Digital Bathymetry (IHO DCDB; https://www.gebco.net/data_and_products/undersea_feature_names/). Several of the oceanic trenches defined in the IHO DCDB's gazetteer are not thought to be associated with present-day plate subduction (see Section 8.32.3).

8.32.3 Where, how deep and how long are oceanic trenches?

Oceanic trenches cover an area of 1.97 million km², and the Pacific Ocean accounts for approximately 80% of all oceanic trenches (Harris et al., 2014). A total of 39 oceanic trenches are named in the IHO DCDB's gazetteer. This chapter considers 38 of them (Table 1), by excluding the Borchgrevink Trench in the Southern Ocean because it was agreed that it is not a Trench but a possible basin or canyon (IOC-IHO/GEBCO, 2005). Most of the oceanic trenches are located along the accretionary and non-accretionary (erosive) plate subduction margins based on Clift and Vannucchi (2004). However, several of the oceanic trenches in the IHO DCDB's gazetteer are (currently) not associated with plate subductions (Fig. 4); for example, the Vema Trench represents a fracture zone on the Mid-Indian Ridge (Heezen and Nafe, 1964). The nature of the crust subducting beneath the western Mediterranean Ridge accretionary complex in the Eastern Mediterranean is long debated. Several evidences suggest the oceanic nature of the subducting crust (Pearce et al., 2012; Kioka et al., 2015; Tugend et al., 2019).

Of the 38 oceanic trenches, 28 are located in the Pacific Ocean generated by the Ring of Fire (Fig. 4). There are no oceanic trenches in the Arctic Ocean in which the deepest water depth is –5669 m (Stewart and Jamieson, 2019). To provide physiographical properties of each oceanic trench the bathymetric data from Kioka et al. (2019a, 2019b) was used for the Japan Trench, Leat et al. (2014, 2016) for the South Sandwich Trench, and GEBCO 2020 Grid (GEBCO Bathymetric Compilation Group, 2020) for the other oceanic trenches. Based on these bathymetric data, the deepest point of the given oceanic trench ranges between –3470 m at the Strabo Trench in the Eastern Mediterranean Sea and –10,950 m at the Mariana Trench in the Pacific Ocean (Table 1) with an average and median of –7160 m and –7290 m, respectively. Some of trenches along the Mediterranean Ridge Accretionary Complex in the Eastern Mediterranean Sea (Ptolemy, Pliny and Strabo Trenches) are shallower than several oceanic troughs such as the Pocklington Trough in the Coral Sea and the Nankai Trough in Japan. Many of the very-deep oceanic trenches are located along erosive plate subduction margins (Clift and Vannucchi, 2004). The deepest point at a given oceanic trench is named; e.g., Vavilov Hole at the Hellenic Trench, Scholl Deep at the Kermadec Trench, Richards Deep at the Peru-Chile (Atacama) Trench, Emden Deep at the Philippine Trench, Horizon Deep at the Tonga Trench and Challenger Deep at the Mariana Trench. The eastern Pacific has only one oceanic trench, Peru-Chile (Atacama) Trench, that represents the deepest point at more than –8 km, while the west Pacific hosts 12 oceanic trenches deeper than –8 km (Table 1), highlighting the striking contrast between trench depths in the east and west Pacific.

The cumulative length of 38 oceanic trenches is approximately 47,900 km, longer than Earth's circumference (Table 1). The length of the respective oceanic trench is calculated by its continuity and the cumulative distance between neighboring deep points along the trench axis extracted at an interval of 0.005° along latitude or longitude from GEBCO 2020 Grid (GEBCO Compilation Group, 2020). Individual trench lengths range between 140 km (Fiordland Trench) and 4900 km (Sunda Trench) with an average and median of 1260 km and 940 km, respectively. Oceanic trenches along the Mediterranean Ridge Accretionary Complex in the Eastern Mediterranean Sea (Hellenic Trench, Pliny Trench, Ptolemy Trench and Strabo Trench) are relatively short and less continuous, ranging between 190 and 430 km. Several oceanic trenches (Aleutian/Kuril-Kamchatka Trenches, Ecuador/Peru Trenches and Peru/Peru-Chile (Atacama) Trenches) are distinguished from others due to facing a triple junction where the boundaries of three plates meet; although they are rather geomorphologically continuous. Moreover, the continuities of several oceanic trenches are punctuated by seamounts currently being subducted (Watts et al., 2010), including Kodiak Seamount at the Aleutian Trench (von Huene et al., 2012), Mogi Seamount at the Izu-Ogasawara (Izu-Bonin) Trench; Daiichi-Kashima Seamount at the Izu-Ogasawara (Izu-Bonin) and Japan Trenches (Mogi and Nishizawa, 1980; Kobayashi et al., 1987), Erimo Seamount at the Japan and Kuril-Kamchatka Trenches (Cadet et al., 1987), Fisher Seamount at the Middle America Trench (von Huene et al., 2000), Capricorn Seamount at the Tonga Trench (Brodie, 1965) and Osbourn Seamount at the Tonga and Kermadec Trenches (Hawkins et al., 1987).

Oceanic trenches are typically 50–100 km in width and form an asymmetric V-shape depression with the steepest surface slope of up to ~10° on the landward slope (Clift and Vannucchi, 2004). The distance from the deepest point of the respective oceanic trench to the closest land is calculated by using a Global Self-consistent, Hierarchical, High-resolution Geography (GSHHG) database version 2.3.7 (Wessel and Smith, 1996). The distance from deepest point to land ranges between 23 and 522 km (Table 1),

Table 1 Properties of oceanic trenches.

Name	Total length (km)	Deepest depth (m)	Longitude of deepest point (degree)	Latitude of deepest point (degree)	Distance to land (km)	Area of water depths < -6000 m (km ²)	Area of water depths < -7000 m (km ²)	Area of water depths < -8000 m (km ²)	Sediment thickness at deepest point (km)	Crustal Age at deepest point (Myr)
Aleutian	3970	-7889	-173.2438	50.7854	135	106,230	29,152	0	0.73	56
Amirante	620	-5260	52.6021	-8.1146	107	0	0	0	0.54	64
Cayman	840	-7323	-79.4563	19.2354	62	8691	1315	0	0.98	30
Cedros	550	-4617	-116.1271	28.0771	57	0	0	0	0.36	13
Chile	930	-4720	-71.9146	-55.9979	113	0	0	0	0.42	19
Colombian	630	-4440	-78.3646	6.5938	78	0	0	0	0.48	12
Ecuador	380	-4578	-81.6146	-2.9688	107	0	0	0	0.36	31
Fiordland	140	-4530	165.7396	-45.6271	56	0	0	0	0.47	58
Hellenic	430	-5124	21.1229	36.5771	54	0	0	0	5.97	247
Hjort	550	-6735	157.6604	-58.2646	364	1298	0	0	0.09	26
Izu-Ogasawara (Izu-Bonin)	1200	-9828	142.8271	29.1396	171	103,838	57,114	28,991	0.13	137
Japan	610	-8035	142.7048	36.0512	169	38,050	11,641	51	0.91	132
Kermadec	1270	-10,101	-177.1854	-31.7646	187	104,845	44,650	20,057	0.20	112
Kuril-Kamchatka	2200	-9707	152.8396	45.2354	188	129,040	59,339	15,530	0.65	116
Mariana	2510	-10,952	142.5896	11.3688	286	140,215	61,085	24,542	0.10	148
Middle America	2830	-6721	-93.5229	13.9104	147	3930	0	0	0.32	26
Nansei-Shoto (Ryukyu)	1380	-7459	125.1354	23.1979	156	42,509	4059	0	0.40	54
New Britain	940	-9246	154.1438	-6.7854	112	30,370	10,419	1800	0.53	38
New Guinea	1230	-5419	135.3063	0.2438	60	0	0	0	0.61	24
North New Hebrides	460	-9122	165.7271	-11.9396	107	8353	3246	1097	0.02	40
Palau	310	-8051	134.9771	7.7354	36	4096	932	104	0.18	45
Peru	1600	-6659	-79.7313	-10.7063	182	6377	0	0	0.40	40
Peru-Chile (Atacama)	4140	-8274	-71.3521	-23.4229	74	49,508	11,873	129	0.10	52
Philippine	1830	-10,198	126.8938	9.5146	79	84,064	38,986	17,084	0.65	76
Pliny	290	-3997	25.4979	34.2771	68	0	0	0	8.52	264
Ptolemy	380	-3623	24.2063	34.6063	23	0	0	0	9.01	266
Puerto Rico	1170	-8555	-65.2438	19.8771	153	86,373	35,335	7513	0.18	105
Puysegur	480	-6296	164.4563	-48.0479	155	475	0	0	0.30	26
South New Hebrides	1330	-7490	172.1563	-23.0896	77	10,348	218	0	0.21	35
South Sandwich	1230	-8182	-24.8271	-56.2777	142	43,650	17,167	357	0.58	61

(Continued)

Table 1 Properties of oceanic trenches.—cont'd

Name	Total length (km)	Deepest depth (m)	Longitude of deepest point (degree)	Latitude of deepest point (degree)	Distance to land (km)	Area of water depths < -6000 m (km ²)	Area of water depths < -7000 m (km ²)	Area of water depths < -8000 m (km ²)	Sediment thickness at deepest point (km)	Crustal Age at deepest point (Myr)
South Solomon	680	-8604	163.0354	-11.2479	75	8561	2558	147	0.02	35
Strabo	190	-3467	26.7188	34.1771	98	0	0	0	10.16	265
Sunda (Java)	4920	-7253	110.3563	-10.3479	242	74,138	1673	0	0.60	120
Tonga	1690	-10,834	-174.7396	-23.2646	182	99,046	46,950	23,043	0.05	88
Vema	240	-6511	67.2563	-9.1354	522	322	0	0	0.02	4
Vityaz	1490	-6188	170.2479	-10.2688	152	473	0	0	0.09	102
West Melanesian (Manus)	1500	-7058	149.3146	-0.4979	95	7094	54	0	0.17	37
Yap	730	-8935	138.6938	10.5479	112	18,419	6475	859	0.09	119
Total	47,870					1,210,313	444,241	141,305		
% of entire seafloor						33.2	94.4	95.2		

The names of oceanic trenches listed here are from the gazetteer at the IHO DCDB (https://www.gebco.net/data_and_products/undersea_feature_names/). The deepest depth and areal extent of water depths of deeper than -6, -7 and -8 km at the respective trench (excl. Japan Trench and South Sandwich Trench) are computed from GEBCO 2020 Grid (GEBCO Compilation Group, 2020). The bathymetric data at the Japan Trench and South Sandwich Trench analyzed here are from Kioka et al. (2019a, b) and Leat et al. (2014, 2016), respectively. The distance from deepest point to land is computed by using a Global Self-consistent, Hierarchical, High-resolution Geography (GSHHG) database version 2.3.7 (Wessel and Smith, 1996). Sediment thickness of a given trench is extracted from GlobSed, a global 5-arc-minute total sediment thickness grid data (Straume et al., 2019). The oceanic crustal age is extracted from a global dataset of present-day oceanic crustal age (Müller et al., 2008; Seton et al., 2020).

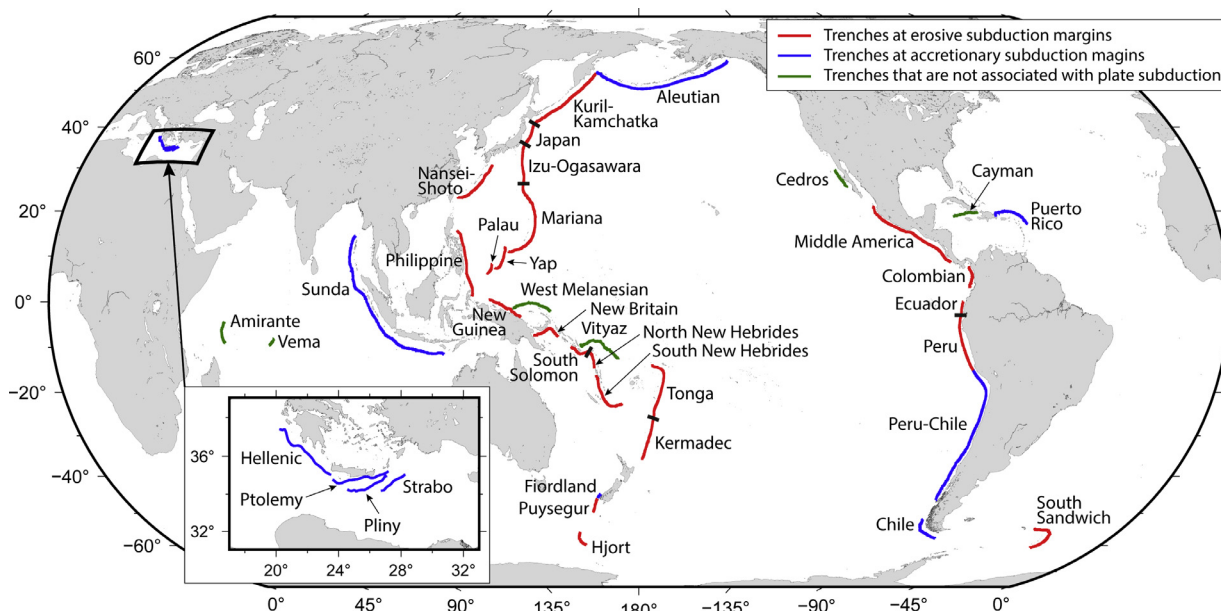


Fig. 4 Oceanic trenches listed in [Table 1](#). Red: Oceanic trenches at erosion-dominant subduction margins; Blue: Oceanic trenches at accretion-dominant subduction margins; Green: Oceanic trenches that are (currently) not associated with plate subductions.

with an average and median of 136 and 112 km, respectively. In general, the distance is longer for the deeper oceanic trench. However, the deepest points at several deep oceanic trenches are relatively close to the land (e.g., Palau Trench; [Kobayashi, 2004](#)), suggesting the landward surface slope of bathymetric relief is very large at these oceanic trenches (see [Section 8.32.5](#)).

8.32.4 Hadal trenches: The deepest places on the Earth's surface

Total surface area of ocean on the Earth is 361.9 million km² in light of GEBCO 2020 Grid ([GEBCO Compilation Group, 2020](#)). Although the seafloors at water depths of < −5 km are widely distributed worldwide, the eastern Tropical Pacific has less area of seafloor deeper than < −5 km, highlighting the contrast between west and east Pacific Ocean ([Fig. 5](#)). The hadal zone (water depths < −6 km) accounts for 45% of the total ocean range (−11–0 km). Yet, its total surface area of the seafloor is 3.64 million km², accounting for only 1.0% of total area of seafloor. Many of the hadal zones are located in the west Pacific Ocean. There are no hadal seafloors in the Arctic Ocean in which the deepest water depth is −5669 m ([Stewart and Jamieson, 2019](#)).

Of the 38 oceanic trenches, 27 have the deepest seafloors within the hadal zone (hadal trenches), and 23 of the hadal trenches are located in the Pacific Ocean ([Fig. 6](#)). The hadal trenches host 33% of total area of hadal seafloor (1.21 million km²; [Table 1](#)). The hadal trenches comprise total areas of 0.44 and 0.14 million km² of hadal seafloors deeper than −7 and −8 km, respectively, accounting for 94% and 95% of the total area of the entire hadal seafloor ([Table 1](#)). Therefore, the hadal trenches are the deepest places on the Earth's surface. Furthermore, the deepest places at the Izu-Ogasawara (Izu-Bonin) Trench, Kermadec Trench, Kuril-Kamchatka Trench, Mariana Trench, New Britain Trench, North New Hebrides Trench, Philippine Trench, Tonga Trench are deeper than −9 km ([Table 1](#)), and thus Mount Everest would fit inside these oceanic trenches.

The study of the hadal zone remains challenging as a result of the extreme hydrostatic pressure, more than 60 MPa, on the seafloor. Hadal trenches are thus the least studied places on the Earth's surface and due to the difficulties in surveying such deep water depths, are even less explored than Earth's Moon and Mars. Better understanding of hadal trenches, however, enhances our understanding of the limit of habitat depth for deep-sea fauna ([Jamieson et al., 2010; Stewart and Jamieson, 2018](#)). Research has unveiled unexpectedly large amounts of carbon matter accumulating in the hadal trenches ([Danovaro et al., 2003; Wenzhoefer et al., 2016; Bao et al., 2018; Luo et al., 2018; Kioka et al., 2019a; Glud et al., 2021](#)), suggesting their pivotal role in the deep carbon cycle. Oceanic trenches are well ventilated because of the overflow of dense water currents ([Johnson, 1998](#)), resulting in supply of oxygen and nutrients to the deep seafloors ([Ichino et al., 2015](#)). The Mariana Trench is found to maintain unexpectedly high levels of microbial activity ([Glud et al., 2013](#)). At the same time, the great depths of oceanic trenches cause tremendous amounts of accumulating microplastics, and consequently persistent organic pollutants; serving as an ultimate trashcan of anthropological origin matters ([Fischer et al., 2015; Shimanaga and Yanagi, 2016; Jamieson et al., 2017; Peng et al., 2020](#)).

Improvements in measuring such ultra-deep-water depths are paralleled with mankind's motivation to improve knowledge of the exact depth of the respective hadal trenches. Since the 1950s many surveys have specifically focused on the Challenger Deep in the Mariana Trench ([Carruthers and Lawford, 1952; Hanson et al., 1959; Fisher and Hess, 1963; Fujioka et al., 2002; Taira et al., 2005; Nakanishi and Hashimoto, 2011; Gardner et al., 2014](#)). In addition to the Mariana Trench, there is an emerging increase

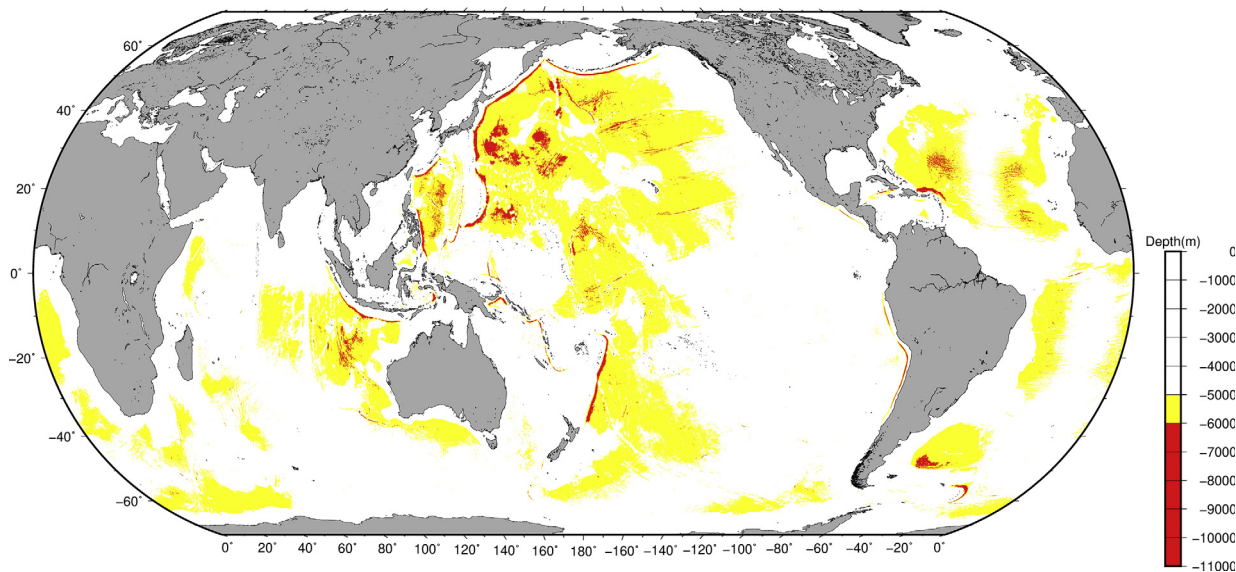


Fig. 5 Areas with seafloors at water depths of 5–6 km (yellow) and 6–11 km (red). Bathymetry data are from GEBCO 2020 Grid (GEBCO Compilation Group, 2020).

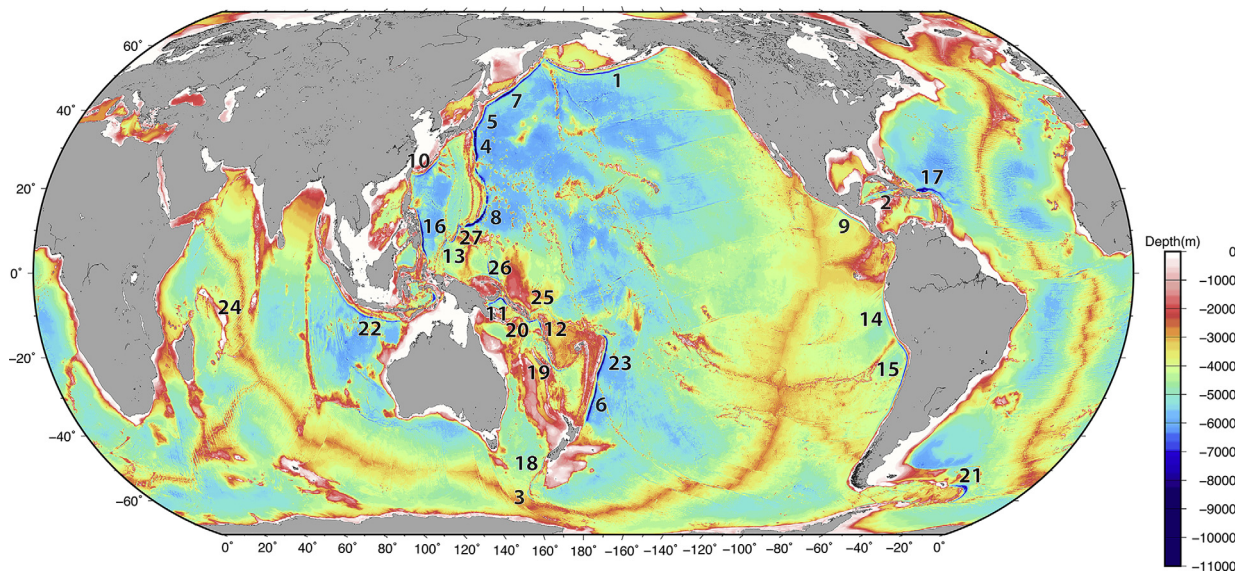


Fig. 6 Hadal trenches. 1: Aleutian Trench; 2: Cayman Trench; 3: Hjort Trench; 4: Izu-Ogasawara (Izu-Bonin) Trench; 5: Japan Trench; 6: Kermadec Trench; 7: Kuril-Kamchatka Trench; 8: Mariana Trench; 9: Middle America Trench; 10: Nansei-Shoto (Ryukyu) Trench; 11: New Britain Trench; 12: North New Hebrides Trench; 13: Palau Trench; 14: Peru Trench; 15: Peru-Chile (Atacama) Trench; 16: Philippine Trench; 17: Puerto Rico Trench; 18: Puysegur Trench; 19: South New Hebrides Trench; 20: South Sandwich Trench; 21: South Solomon Trench; 22: Sunda (Java) Trench; 23: Tonga Trench; 24: Vema Trench (fracture zone); 25: Vityaz Trench; 26: West Melanesian (Manus) Trench; 27: Yap Trench. Bathymetry data are from GEBCO Compilation Group (2020).

in the number of research cruises to other hadal trenches in the last two decades (Jamieson, 2018), with likely more than 5 hadal research cruises annually since 2011. They have also highlighted the significant uncertainty in estimating depth and location of deepest place mainly due to the measurement uncertainty, precise sound velocity estimation and data processing in the multibeam echosounder data. Likewise, for all the other oceanic trenches, the depth and exact location in the respective oceanic trench is currently undetermined (Stewart and Jamieson, 2019); thus both acquisition of high-density and high-resolution bathymetric data as well as sound velocity measurements and conductivity-temperature-depth profiler (CTD) casts are crucial for better characterizing oceanic trench geomorphologies.

8.32.5 What controls the depth of seafloor at an oceanic trench?

A better understanding of the geomorphological nature of oceanic trenches, including how and why they are deep, will advance the understanding of the evolutionary processes and dynamics of the solid earth. As briefly reviewed in Sections 8.32.3 and 8.32.4, the deepest point in a given oceanic trench varies between trenches, ranging between –3470 m at the Strabo Trench to –10,950 m at the Mariana Trench (Table 1). Most of the hadal trenches are located in the Pacific Oceans. This may encourage us to ask a question like “what does determine the depth of seafloor at each oceanic trench?” The deepness of the given oceanic trench could be primarily controlled by (1) the sediment influx from land and the continental slope and (2) the age of the subducting oceanic lithosphere as suggested by Parsons and Sclater (1977) and Stein and Stein (1992). This section thus briefly reviews the relationships between the sediment thickness, crustal age and depth at the deepest points within a specific oceanic trench.

Sediment thickness at the given oceanic trench is extracted from GlobSed, a global 5-arc-minute total sediment thickness data grid which is compiled from seismic reflection and refraction data (Straume et al., 2019). The sediment thickness at the deepest point of the respective oceanic trench ranges from 0.02 km (e.g., North New Hebrides and South Solomon Trenches) to 10.16 km (Strabo Trench); with an average and median of 1.20 and 0.38 km, respectively (Table 1). Sediment thickness could be the main factor that influences the water depth at an oceanic trench because the trench depression can be filled by sediment supply from the adjacent continental areas and continental slope. However, there is no clear relationship between water depth and sediment thickness (Fig. 7A). This is partly due to the different settings and magnitudes of sediment supply that result in the geomorphologically-different trench depressions. For example, the oceanic trenches in the Mediterranean Ridge Accretionary Complex (Hellenic Trench, Pliny Trench, Ptolemy Trench and Strabo Trench), yield the thickest sediment deposits at the trench; including thick Messinian evaporites sequences (Reston et al., 2002), which result in a rather vague expression of the bathymetric features of the trench depressions. In addition, the abundant sediment supply and substantial sediment transport toward greater depths, smooths the bathymetric features of the trench depression making them unrecognizable in present-day bathymetry. Examples of this are the Makran “trench” and Cascadia “trench” with a maximum sediment thickness of 7.5 and 4 km, respectively (Flueh et al., 1998; Kopp et al., 2000; Smith et al., 2012). This may also explain why the cumulative length of oceanic trenches is shorter than that of present-day convergent plate margins (~77%; 47,900 km out of 61,900 km).

As newly formed oceanic lithosphere moves away from a mid-ocean ridge, it is cooled and contracts and increases in density. The depth of oceanic trenches may thus be primarily controlled by the age of the subducting oceanic lithosphere, because it determines the degree of bending of the plate and the depth to the oceanic crust entering the trench (i.e., an older (colder) plate subducts at a steeper degree). In addition, the age of oceanic lithosphere determines the amount of pelagic sediment accumulated on the oceanic basement (i.e., an older plate has more time to accumulate thicker pelagic sediment on the basement). The age of oceanic lithosphere being subducted at a given oceanic trench can be extracted from a global dataset of present-day oceanic crustal age (Müller et al., 2008; Seton et al., 2020). The age of oceanic lithosphere at the deepest point of the given oceanic trench ranges between 4 and 266 million years (Myr) with an average and median of 82 and 55 Myr, respectively (Table 1). There is a general trend of deeper oceanic trenches with older subducting oceanic lithosphere as expected (Fig. 7B). The contrast between trench depths in the east and west Pacific might partly be explained by the systematic difference in the age of subducting oceanic lithosphere.

Yet, the crustal age alone cannot fully explain the depth of each oceanic trench. Prominent examples are the oceanic trenches in the Mediterranean Ridge Accretionary Complex that represent very shallow water depths given the older age of subducting crust (Fig. 7B). We thus subtracted the sediment thickness from the present-day water depth, taking into account isostatic correction, to estimate the sediment-bare basement depth at the deepest point of the respective oceanic trench. This depth was computed using a global 5-arc-minute total sediment thickness grid data GlobSed (Straume et al., 2019) and an empirical formulation for isostatic correction (Sykes, 1996). There is a good correlation between the sediment-bare basement depth and age of oceanic lithosphere subducted at the deepest point of the respective oceanic trench in the plate subduction margin; i.e., the sediment-bare basement depth is greater when the age is older (Fig. 8). This suggests the combination of age of oceanic lithosphere and sediment thickness is a primary factor that determines the water depth of oceanic trench.

Having said that, several oceanic trenches at the plate subduction margins deviate from the correlation between the sediment-bare depth and age of oceanic lithosphere. For example, the New Britain Trench, North New Hebrides Trench, Palau Trench, Philippine Trench and South Solomon Trench yield younger ages of subducting oceanic lithosphere than expected from their sediment-bare basement depth (Fig. 8). Such deviations could partly be explained by the surface slope of bathymetric relief and dip angle of subduction. Fig. 9 shows water depth at distance from the trench axis and surface slope of bathymetric relief of the given oceanic trench computed from GEBCO 2020 Grid (GEBCO Compilation Group, 2020). The oceanic trenches at the accretionary margins such as the Aleutian and Chile Trenches are characterized with low surface slope as suggested by Clift and Vannucchi (2004) and Polonia et al. (2007). On the other hand, the Palau Trench, Philippine Trench and South Solomon Trench represent remarkably large landward surface slopes, making the sediment-bare basement depth deeper than anticipated from their age of oceanic lithosphere. The New Britain and North New Hebrides Trenches have larger subduction angles than expected from their young age of oceanic lithosphere (Heuret et al., 2011). These features are also strongly related to the flexure of the subducting lithosphere at an oceanic trench due to the vertical force and bending moment (Turcotte et al., 1978).

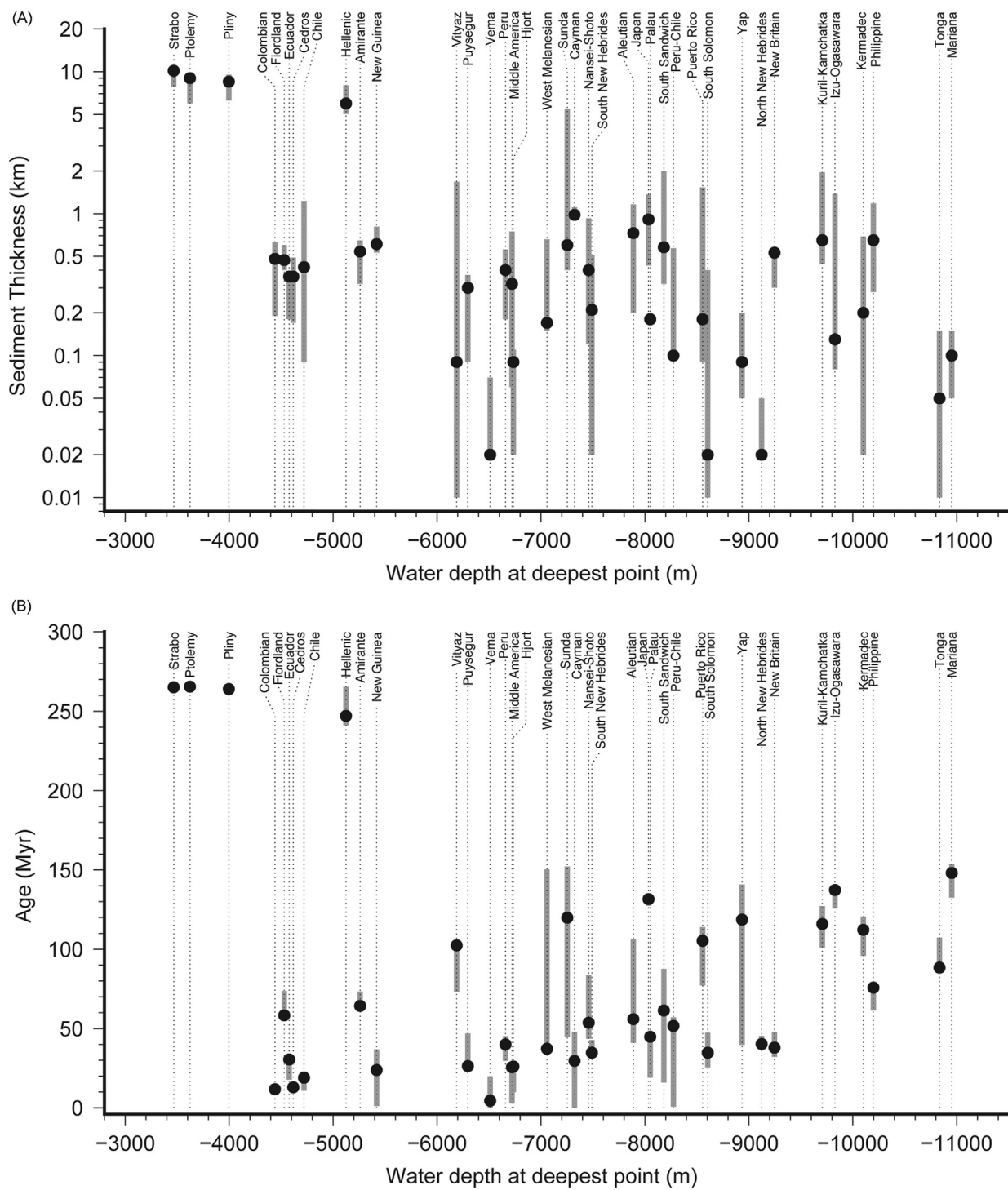


Fig. 7 (A) Water depth of deepest seafloor versus sediment thickness of the given oceanic trench. Black circles indicate the sediment thickness at the deepest point of the given oceanic trench and the gray lines indicate the thickness along the entire trench axis. The data for sediment thickness are from Straume et al. (2019). (B) Water depth of deepest seafloor versus present-day oceanic crustal age of a given oceanic trench. Black circles and gray lines indicate the crustal age at the deepest point of the given oceanic trench and that along the entire trench axis of the given oceanic trench, respectively. The data of oceanic crustal age are from Müller et al. (2008) and Seton et al. (2020).

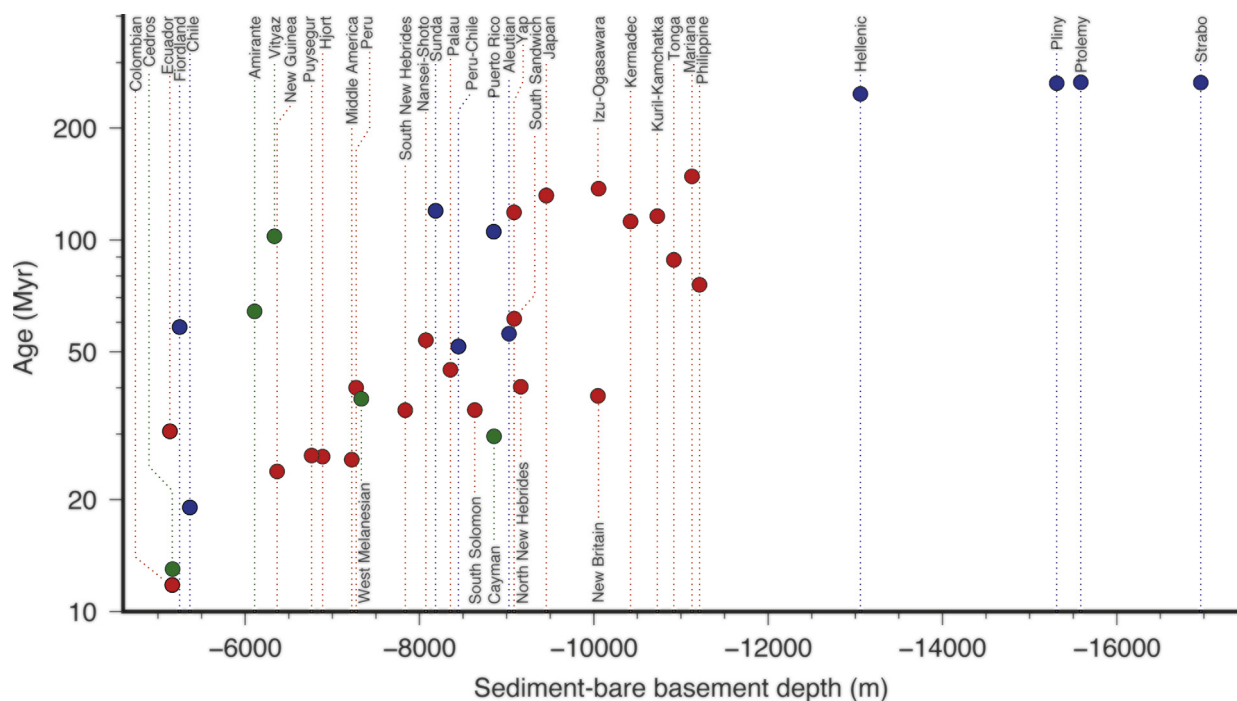


Fig. 8 Sediment-bare basement depth versus present-day crustal age at the deepest point of the given oceanic trench. Red: Oceanic trenches at erosive subduction margins; Blue: Oceanic trenches at accretionary subduction margins; and Green: Oceanic trenches that are not associated with plate subductions.

8.32.6 Isolated depositional basins at the trench axis floor

Many surveys to acquire bathymetric and reflection seismic data at deep oceanic trenches were performed in response to megathrust earthquakes in the last two decades. For example, the Japan Trench, where the giant 2011 Tohoku-oki Earthquake occurred, has been heavily studied for better characterization of horst-and-graben topography, and large coseismic slips and resulting deformation at the trench (Fujiwara et al., 2011, 2017; Kodaira et al., 2012; Nakamura et al., 2013; Strasser et al., 2013). Conventionally, the seafloor along the trench axis was thought to be characterized by the V-shaped depression structures with very steep landward and seaward slopes. However, knowledge gained about trench sedimentation, by piston cores in combination with recently acquired high-resolution bathymetric data and hydroacoustic data (sub-bottom profiler data), has revealed that the hadal Japan trench system hosts many flat, isolated depositional basins (Ikehara et al., 2016, 2018; Kioka et al., 2019a, b; Schwestermann et al., 2020; McHugh et al., 2020). Studies show around 40 small, isolated trench-fill basins, the area of the largest of which is 29 km², along a 600 km-long trench axis (Fig. 10). With the help of the highest resolution bathymetry data currently available, Kioka et al. (2019b) attempted, for the first time, to identify the pathways of sediment transport from land to the deep and to estimate flow accumulation (Fig. 10). Their estimation suggested that funneling and focusing of sediment density flows through the two submarine canyons in the southernmost and northernmost Japan Trench, Nakaminato canyon and Ogawara canyon, respectively; transports a large amount of sediment from land and continental slopes into the proximal basins. These results highlight the heterogeneity of water depths along the trench axis as influenced by the nature of the horst-and-graben structure and the different magnitudes of sediment supply to the individual basins.

The new findings in the Japan Trench raises the question “Do other oceanic trenches also comprise flat, isolated depositional basins at the trench floor?” If yes, it is worth studying such basins in greater detail because they could serve as the ultimate sink of materials on the Earth’s surface. To assess whether oceanic trenches have trench-fill basins along their axes, the relief roughness coefficient was computed using the Melton ruggedness number (Melton, 1965) to highlight relative level relief (Figs. 11 and 12). The lower relief roughness coefficient means more gentle undulating bathymetry at the point of interest, indicative of a possible trench-fill basin at the given point. For example, the places with low relief roughness coefficients correspond to the trench-fill basins identified by piston coring and sub-bottom profiler data in the Japan Trench. The large areal extents of places with a low relief roughness coefficient in the southernmost and northernmost Japan Trench correspond with the largest isolated trench-fill basins (JTS01 and JTN08; Fig. 11). Given that the relief roughness coefficient can highlight the places of trench-fill basins at the Japan Trench, other oceanic trenches can be studied to seek similar basins in light of GEBCO 2020 Grid, where sufficient resolution data are available. For example, when looking at the deepest points of the Kermadec Trench, Kuril-Kamchatka

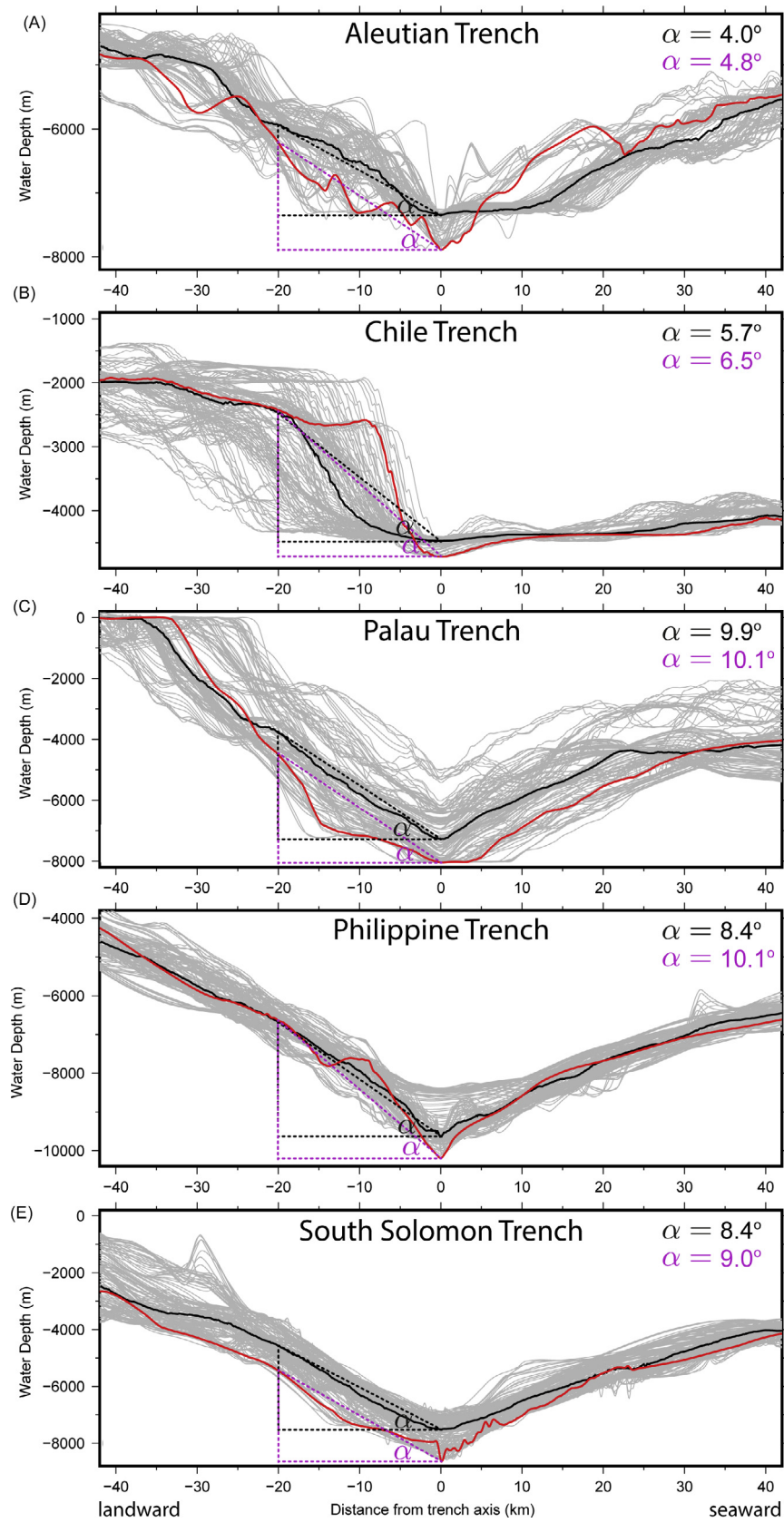


Fig. 9 Water depth at the distance from the trench axis and surface slope of bathymetric relief (α) of the given oceanic trench computed from GEBCO 2020 Grid (GEBCO Compilation Group, 2020). Gray thin lines show the profiles within the 1° window from the deepest point of the given trench. The black line shows its median profile. The red line shows the profile across the deepest point of the given trench. The surface slope (α) is estimated from differences in water depths between 0 and -20 km in distance from the trench axis.

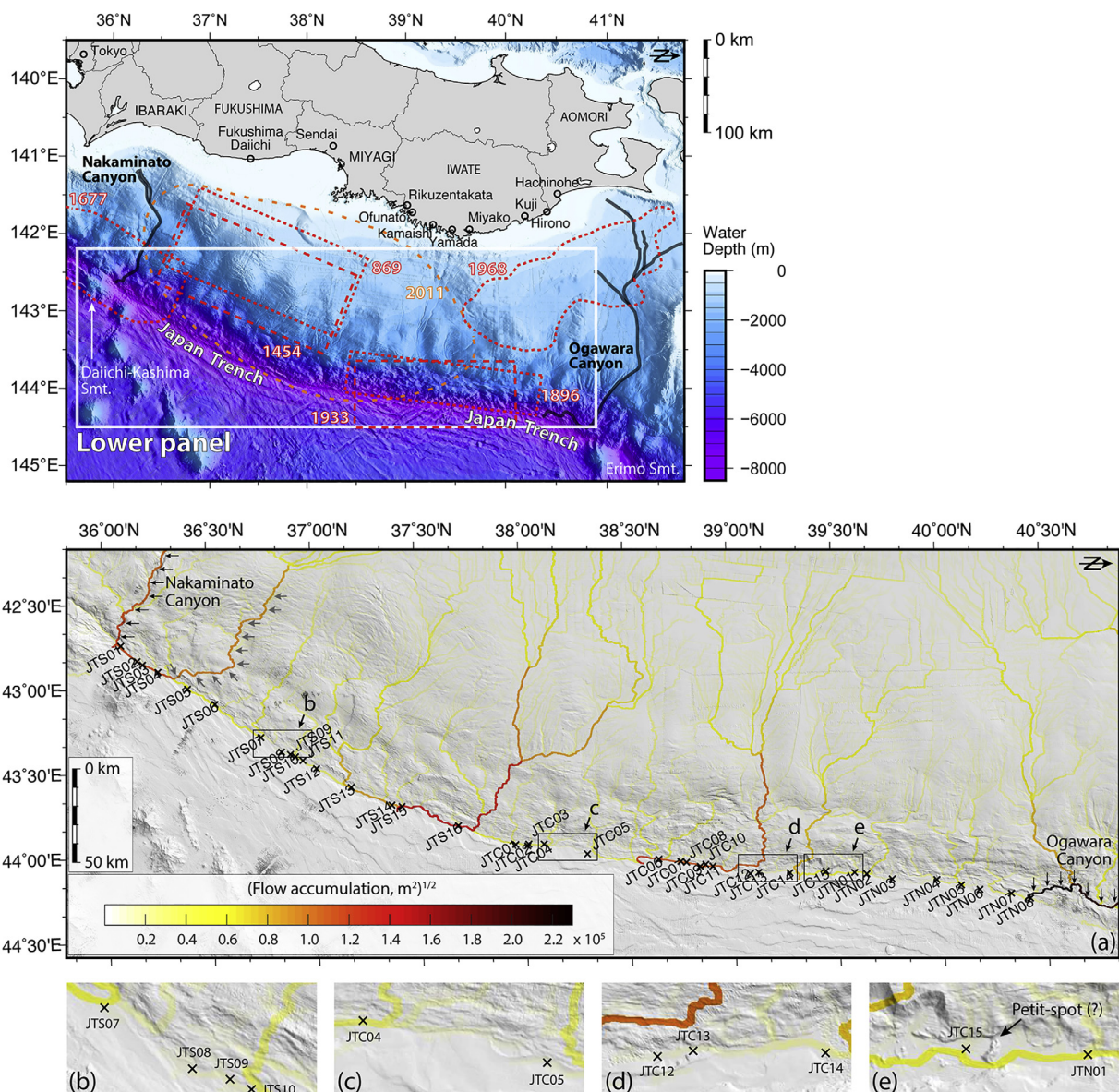


Fig. 10 (Upper panel) Map of the Japan Trench with the zones of seismic rupture and slips of historically known large earthquakes (see Kioka et al. (2019b) and reference therein). (Lower panel) Flow accumulation in the Japan Trench (Kioka et al., 2019b). Modified from Kioka A, Schwestermann T, Moernaut J, Ikehara K, Kanamatsu T, Eglinton TI, Strasser M (2019b). Event stratigraphy in a Hadal Oceanic Trench: The Japan Trench as sedimentary archive recording recurrent giant subduction zone earthquakes and their role in organic carbon export to the deep sea. *Frontiers in Earth Science* 7: 319, doi:10.3389/feart.2019.00319.

Trench, Peru-Chile (Atacama) Trench, Pliny Trench, Puerto Rico Trench and Sunda (Java) Trench, low relief roughness coefficients are found, suggesting the existence of possible trench-fill basins (Fig. 12). Their areal extent may be comparable to those identified at the Japan Trench. The deepest point at the Hellenic Trench also represents a small and relatively flat basin, known as the Vavilov Hole. Although further high-resolution bathymetric surveys combined with piston coring and dense hydroacoustic data are necessary, the bathymetry data currently available alone suggests the possible presence of flat, isolated trench-fill basin at each oceanic trench.

8.32.7 Conclusion

This chapter presents an overview of global and local features of oceanic trenches to provide readers with an introduction and a starting point for more in-depth geomorphological studies on oceanic trenches. Most of the oceanic trenches named in the IHO DCDB's

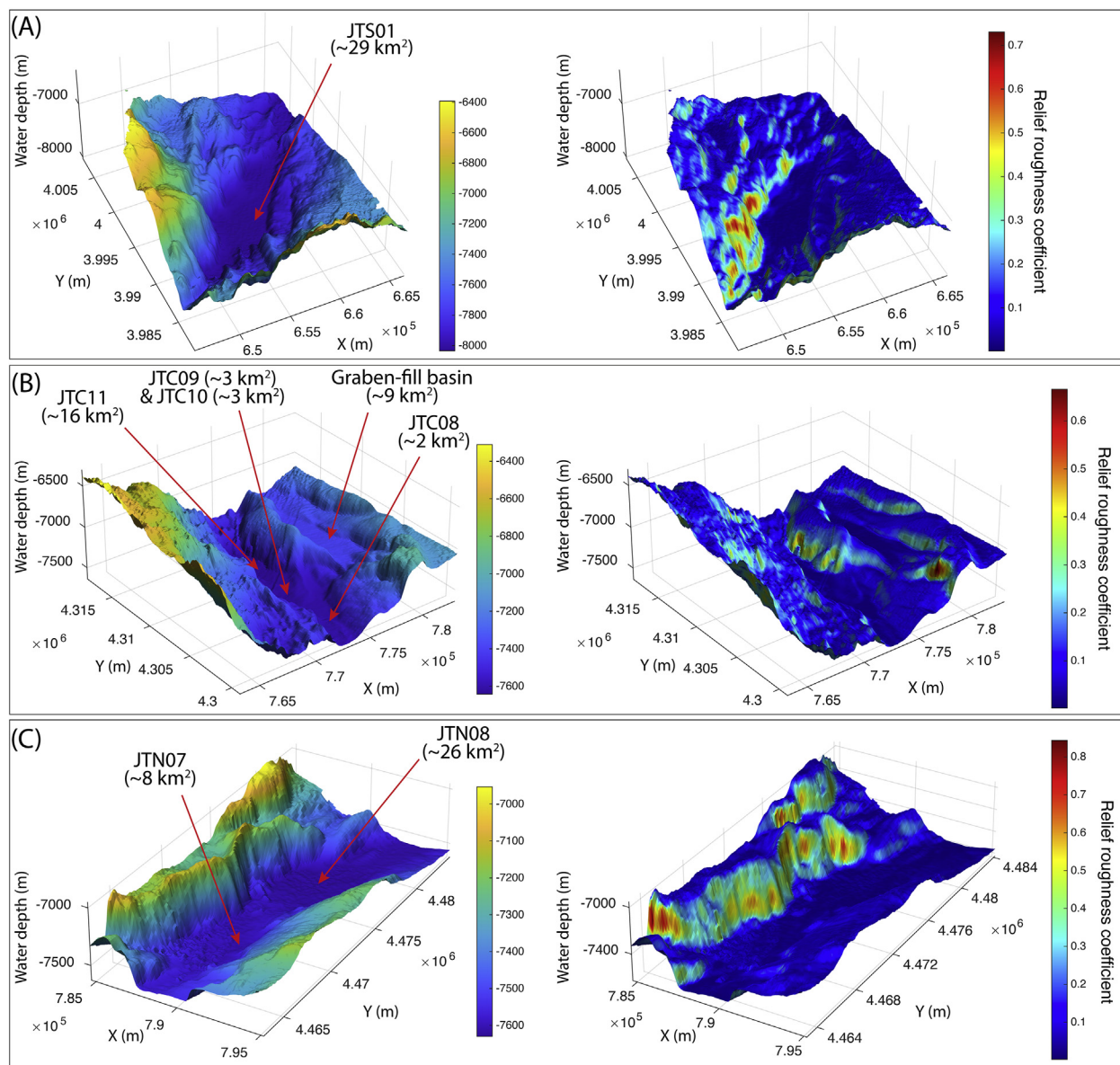


Fig. 11 High-resolution bathymetry and relief roughness coefficient at trench-fill basins in the Japan trench. Bathymetry data are from Kioka et al. (2019a, 2019b). (A) Southernmost trench-fill basin JTS01 is located at the deepest point of the Japan Trench (see Fig. 9 for the location). (B) Central trench-fill basins JTC08–JTC11 (see Fig. 9 for the locations). (C) Northernmost basins JTN07 and JTN08 (see Fig. 9 for the locations). Red arrows indicate the points of depocenters for the respective basins. The areal data are from Kioka et al. (2019b).

gazetteer are associated with plate subduction, and their total length is approximately 48,000 km. Of the 38 oceanic trenches, 27 are the hadal trenches with their deepest points deeper than -6 km, and most of them are located along the erosive subduction margins. The hadal trenches accommodate 33% of the entire hadal depths of the seafloor and occupy 94% and 95% of the entire seafloor with water depths of <-7 km and <-8 km, respectively. The depth of an oceanic trench is generally explained by the present-day age of subducting oceanic lithosphere while taking into account the sediment thickness and isostatic correction at the oceanic trench. Recent high-resolution bathymetric surveys have revealed that oceanic trenches do not always show the V-shaped depression structures with very steep landward and seaward slopes, and that several trenches have flat floors with small individual depositional basins. For example, Japan Trenches have around 40 small, isolated basins of this sort. In the light of GEBCO 2020 Grid, several other oceanic trenches also locally include flat floors, perhaps with isolated small trench-fill basins along the trench axis at least at its deepest point. This chapter highlights the importance of further, detailed surveys that include acquisition of bathymetric and hydroacoustic data and sediment cores. These are absolutely essential to better understand the geomorphology of the deepest trench floors – the last frontier on the Earth's surface.

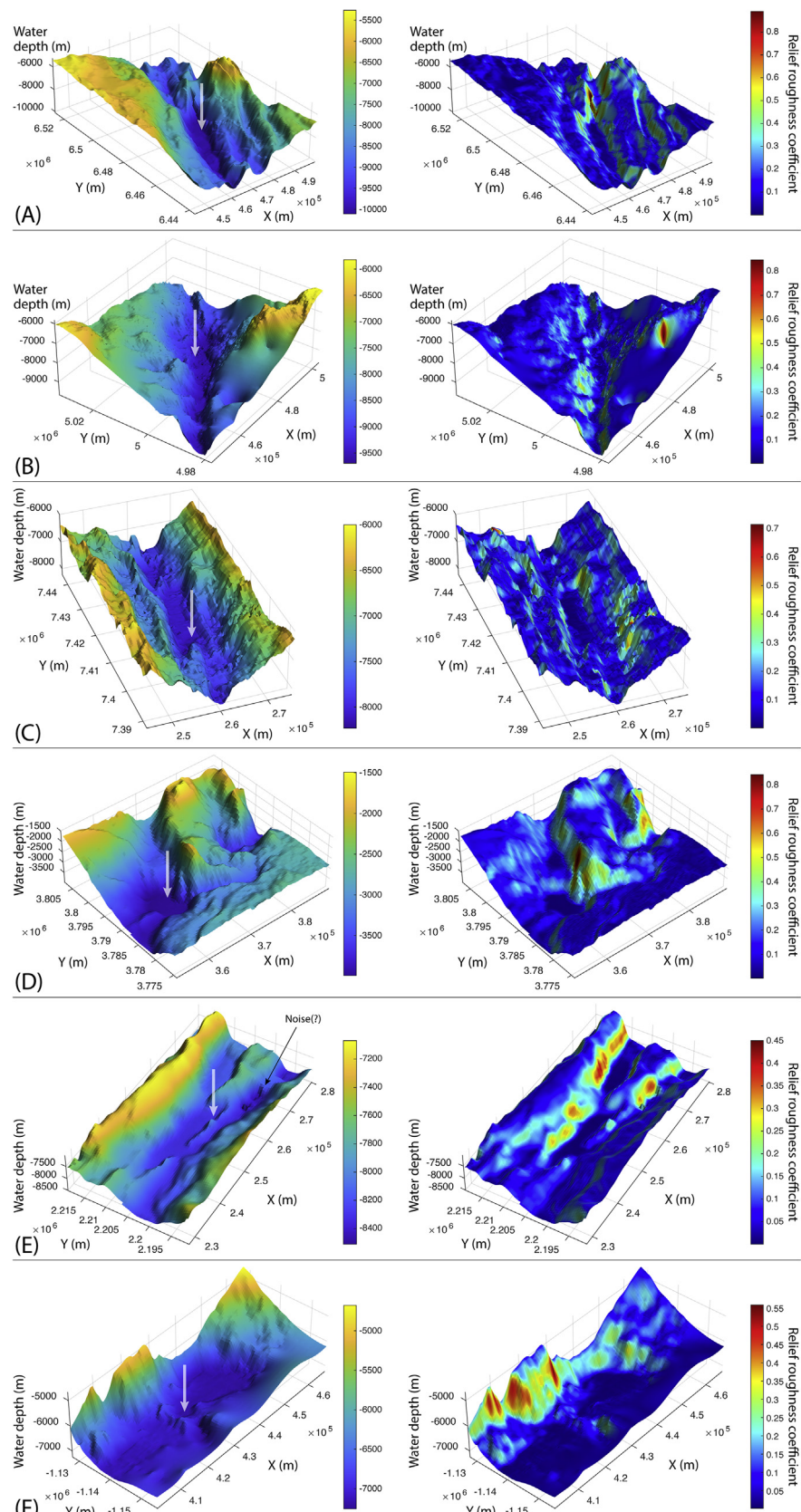


Fig. 12 Deepest places at these oceanic trenches that may represent isolated flat trench-fill basins suggested from the GEBCO 2020 Grid (GEBCO Compilation Group, 2020). Left and right figures show 3-D bathymetry and the relief roughness coefficient for the given trenches. White arrows show the deepest points of each trench. (A) Kermadec Trench. (B) Kuril-Kamchatka Trench. (C) Peru-Chile Trench. (D) Pliny Trench. (E) Puerto Rico Trench. (F) Sunda Trench.

Acknowledgments

A.K. is grateful to Doug Sherman for providing the opportunity for writing this chapter. DEM data were analyzed and mapped by using GMT – Generic Mapping Tools ([Wessel et al., 2019](#)) and TopoToolbox ([Schwanghart and Scherler, 2014](#)). The computation was partly performed on the ITO supercomputer system at the Research Institute for Information Technology, Kyushu University. This work was supported by Austria Science Fund (FWF-P29678) and JSPS Bilateral Joint Research Project (JPJSBP120214811).

References

- Bao, R., Strasser, M., McNichol, A.P., Haghipour, N., McIntyre, C., Wefer, G., Eglington, T.I., 2018. Tectonically-triggered sediment and carbon export to the Hadal zone. *Nature Communications* 9, 121. <https://doi.org/10.1038/s41467-017-02504-1>.
- Bassett, D., Watts, A.B., 2015. Gravity anomalies, crustal structure, and seismicity at subduction zones: 1. Seafloor roughness and subducting relief. *Geochemistry, Geophysics, Geosystems* 16, 1508–1540. <https://doi.org/10.1002/2014GC005684>.
- Bird, P., 2003. An updated digital model of plate boundaries. *Geochemistry, Geophysics, Geosystems* 4, 1027. <https://doi.org/10.1029/2001GC000252>.
- Brodie, J.W., 1965. Capricorn Seamount, south-west Pacific Ocean. *Transactions of the Royal Society of New Zealand* 3 (10), 151–185.
- Cadet, J.P., Kobayashi, K., Lallemand, S., Jolivet, L., Aubouin, J., Boulègue, J., Dubois, J., Hotta, H., Ishii, T., Konishi, K., Niitsuma, N., Shimamura, H., 1987. Deep scientific dives in the Japan and Kuril Trenches. *Earth and Planetary Science Letters* 83, 313–328. [https://doi.org/10.1016/0012-821X\(87\)90074-4](https://doi.org/10.1016/0012-821X(87)90074-4).
- Carruthers, J.N., Lawford, A.L., 1952. The deepest oceanic sounding. *Nature* 169, 601–603. <https://doi.org/10.1038/169601a0>.
- Clift, P., Vannucchi, P., 2004. Controls on tectonic accretion versus erosion in subduction zones: Implications for the origin and recycling of the continental crust. *Reviews of Geophysics* 42, RG2001. <https://doi.org/10.1029/2003RG000127>.
- Danovaro, R., Della Croce, N., Dell'Anno, A., Pusceddu, A., 2003. A depocenter of organic matter at 7800m depth in the SE Pacific Ocean. *Deep Sea Research Part I: Oceanographic Research Papers* 50, 1411–1420. <https://doi.org/10.1016/j.dsr.2003.07.001>.
- Dierssen, H.M., Theberge Jr., A.E., 2016. Bathymetry: Seafloor mapping history. In: *Encyclopedia of Natural Resources: Water*. CRC Press, pp. 644–648. <https://doi.org/10.1081/E-ENRW-120047531>.
- Ferguson, R.L., Hare, T.M., Laura, J., 2018. HRSC and MOLA Blended Digital Elevation Model at 200m v2. Astrogeology PDS Annex. U.S. Geological Survey. http://bit.ly/HRSC_MOLA_Bland_v0.
- Fischer, V., Elsner, N.O., Brenke, N., Schwabe, E., Brandt, A., 2015. Plastic pollution of the Kuril–Kamchatka Trench area (NW pacific). *Deep Sea Research Part II: Topical Studies in Oceanography* 111, 399–405. <https://doi.org/10.1016/j.dsrt.2014.08.012>.
- Fisher, R.L., Hess, H.H., 1963. Trenches. In: Hill, M.N. (Ed.), *The Sea*, vol. 3. Wiley, New York, pp. 411–436.
- Flueh, E.R., Fisher, M.A., Bialas, J., Childs, J.R., Klaeschen, D., Kukowski, N., Parsons, T., Scholl, D.W., Ten Brink, U., Tréhu, A.M., Vidal, N., 1998. New seismic images of the Cascadia subduction zone from cruise SO108—ORWELL. *Tectonophysics* 293, 69–84. [https://doi.org/10.1016/S0040-1951\(98\)00091-2](https://doi.org/10.1016/S0040-1951(98)00091-2).
- Forbes, E., 1844. Report on the Mollusca and Radiata of the Aegean Sea, and their distribution, considered as bearing on geology. *Report of the British Association for the Advancement of Science* for 1843, 130–193.
- Frank, F.C., 1968. Curvature of island arcs. *Nature* 220, 363. <https://doi.org/10.1038/220363a0>.
- Fryer, P., Husson, D.M., 1981. Seafloor spreading in the Mariana trough: Results of Leg 60 drill site selection surveys. In: Husson, D.M., Uyeda, S. (Eds.), *Initial Reports of the Deep Sea Drilling Project*, 60. U.S. Government Printing Office, pp. 45–55. <https://doi.org/10.2973/dsdproc.60.103.1982>.
- Fujii, Y., Satake, K., Sakai, S., Shinohara, M., Kanazawa, T., 2011. Tsunami source of the 2011 off the Pacific coast of Tohoku Earthquake. *Earth, Planets and Space* 63, 815–820. <https://doi.org/10.5047/eps.2011.06.010>.
- Fujioka, K., Okino, K., Kanamatsu, T., Ohara, Y., 2002. Morphology and origin of the Challenger Deep in the Southern Mariana Trench. *Geophysical Research Letters* 29. <https://doi.org/10.1029/2001GL013595>, 10-1–10-4.
- Fujiiwara, T., Kodaira, S., No, T., Kaiho, Y., Takahashi, N., Kaneda, Y., 2011. The 2011 Tohoku-Oki earthquake: Displacement reaching the trench axis. *Science* 334, 1240. <https://doi.org/10.1126/science.1211554>.
- Fujiwara, T., dos Santos Ferreira, C., Bachmann, A.K., Strasser, M., Wefer, G., Sun, T., Kanamatsu, T., Kodaira, S., 2017. Seafloor Displacement After the 2011 Tohoku-oki earthquake in the Northern Japan trench examined by repeated bathymetric surveys. *Geophysical Research Letters* 44, 11833–11839. <https://doi.org/10.1002/2017GL075839>.
- Gardner, J.V., Armstrong, A.A., Calder, B.R., Beaudoin, J., 2014. So, how deep is the Mariana Trench? *Marine Geodesy* 37, 1–13. <https://doi.org/10.1080/01490419.2013.837849>.
- GEBCO Bathymetric Compilation Group, 2020. The GEBCO_2020 Grid—A Continuous Terrain Model of the Global Oceans and Land. British Oceanographic Data Centre, National Oceanography Centre, NERC, UK.
- Glud, R.N., Wenzhöfer, F., Middelboe, M., Oguri, K., Turnewitsch, R., Canfield, D.E., Kitazato, H., 2013. High rates of microbial carbon turnover in sediments in the deepest oceanic trench on Earth. *Nature Geoscience* 6, 284–288. <https://doi.org/10.1038/ngeo1773>.
- Glud, R.N., Berg, P., Thamdrup, B., Larsen, M., Stewart, H.A., Jamieson, A.J., Glud, A., Oguri, K., Sanei, H., Rowden, A.A., Wenzhöfer, F., 2021. Hadal trenches are dynamic hotspots for early diagenesis in the deep sea. *Communications Earth & Environment* 2, 21. <https://doi.org/10.1038/s43247-020-00087-2>.
- Golombok, M.P., Phillips, R.J., 2010. Mars tectonics. In: Watters, T.R., Schultz, R.A. (Eds.), *Planetary Tectonics*. Cambridge University Press, Cambridge, pp. 183–232. <https://doi.org/10.1017/CBO9780511691645.006>.
- Griggs, D.T., 1939. A theory of mountain-building. *American Journal of Science* 237, 611–650. <https://doi.org/10.2475/ajs.237.9.611>.
- Hanson, P.P., Zendeovich, N.L., Sergeev, U.V., Udinstev, B.B., 1959. Maximum depths of the Pacific Ocean. *Priroda* 6, 84–88 (in Russian).
- Harris, P.T., Macmillan-Lawler, M., Rupp, J., Baker, E.K., 2014. Geomorphology of the oceans. *Marine Geology* 352, 4–24. <https://doi.org/10.1016/j.margeo.2014.01.011>.
- Hawkins, J.W., Lonsdale, P.F., Batiza, R., 1987. Petrologic evolution of the Louisville seamount chain. In: Keating, B.H., Fryer, P., Batiza, R., Boehlert, G.W. (Eds.), *Seamounts, Islands, and Atolls*, pp. 235–254. <https://doi.org/10.1029/GM043p0235>.
- Heezen, B.C., Nafe, J.E., 1964. Vema trench: Western Indian Ocean. *Deep Sea Research and Oceanographic Abstracts* 11, 79–84. [https://doi.org/10.1016/0011-7471\(64\)91083-6](https://doi.org/10.1016/0011-7471(64)91083-6).
- Heuret, A., Lallemand, S., Funiciello, F., Piromallo, C., Faccenna, C., 2011. Physical characteristics of subduction interface type seismogenic zones revisited. *Geochemistry, Geophysics, Geosystems* 12, Q01004. <https://doi.org/10.1029/2010GC003230>.
- Hjort, J., 1910. The “Michael Sars” North Atlantic Deep-Sea Expedition, 1910. *Nature* 85, 52–55. <https://doi.org/10.1038/085052a0>.
- Ichino, M.C., Clark, M.R., Drazen, J.C., Jamieson, A., Jones, D.O.B., Martin, A.P., Rowden, A.A., Shank, T.M., Yancey, P.H., Ruhl, H.A., 2015. The distribution of benthic biomass in hadal trenches: A modelling approach to investigate the effect of vertical and lateral organic matter transport to the seafloor. *Deep-Sea Research Part I: Oceanography Research Paper* 100, 21–33. <https://doi.org/10.1016/j.dsr.2015.01.010>.
- IHO, 2008. Standardization of Undersea Feature Names: Guidelines Proposal Form Terminology, Edition 4. International Hydrographic Organization and Intergovernmental Oceanographic Commission, Monaco.
- IHO, 2019. Standardization of Undersea Feature Names: Guidelines Proposal Form Terminology, Edition 4.2.0 – October 2019. International Hydrographic Organization, Monaco.

- Ikehara, K., Kanamatsu, T., Nagahashi, Y., Strasser, M., Fink, H., Usami, K., Irino, T., Wefer, G., 2016. Documenting large earthquakes similar to the 2011 Tohoku-oki earthquake from sediments deposited in the Japan Trench over the past 1500 years. *Earth and Planetary Science Letters* 445, 48–56. <https://doi.org/10.1016/j.epsl.2016.04.009>.
- Ikehara, K., Usami, K., Kanamatsu, T., Arai, K., Yamaguchi, A., Fukuchi, R., 2018. Spatial variability in sediment lithology and sedimentary processes along the Japan Trench: Use of deep-sea turbidite records to reconstruct past large earthquakes. *Geological Society of London* 456, 75–89. <https://doi.org/10.1144/SP456.9>.
- IOC-IHO/GEBCO, 2005. Undersea Feature Names in the Ross Sea—IHB Comments. SCUFN18-8.2A. International Hydrographic Bureau, Monoco.
- Jamieson, A., 2015. The Hadal Zone. Cambridge University Press, Cambridge. <https://doi.org/10.1017/CBO9781139061384>.
- Jamieson, A.J., 2018. A contemporary perspective on hadal science. *Deep Sea Research Part II: Topical Studies in Oceanography* 155, 4–10. <https://doi.org/10.1016/j.dsr2.2018.01.005>.
- Jamieson, A.J., Fujii, T., Mayor, D.J., Solan, M., Priede, I.G., 2010. Hadal trenches: The ecology of the deepest places on Earth. *Trends in Ecology & Evolution* 25, 190–197. <https://doi.org/10.1016/j.tree.2009.09.009>.
- Jamieson, A.J., Malkocs, T., Pierney, S.B., Fujii, T., Zhang, Z., 2017. Bioaccumulation of persistent organic pollutants in the deepest ocean fauna. *Nature Ecology and Evolution* 1, 0051. <https://doi.org/10.1038/s41559-016-0051>.
- Johnson, G.C., 1998. Deep water properties, velocities, and dynamics over ocean trenches. *Journal of Marine Research* 56, 329–347. <https://doi.org/10.1357/00224098321822339>.
- Kioka, A., Ashi, J., Sakaguchi, A., Sato, T., Muraoka, S., Yamaguchi, A., Hamamoto, H., Wang, K., Tokuyama, H., 2015. Possible mechanism of mud volcanism at the prism-backstop contact in the western Mediterranean Ridge Accretionary Complex. *Marine Geology* 363, 52–64. <https://doi.org/10.1016/j.margeo.2015.01.014>.
- Kioka, A., Schwestermann, T., Moernaut, J., Ikehara, K., Kanamatsu, T., McHugh, C.M., dos Santos Ferreira, C., Wiemer, G., Haghipour, N., Kopf, A.J., Eglinton, T.I., Strasser, M., 2019a. Megathrust earthquake drives drastic organic carbon supply to the Hadal trench. *Scientific Reports* 9, 1553. <https://doi.org/10.1038/s41598-019-38834-x>.
- Kioka, A., Schwestermann, T., Moernaut, J., Ikehara, K., Kanamatsu, T., Eglinton, T.I., Strasser, M., 2019b. Event stratigraphy in a Hadal Oceanic Trench: The Japan Trench as sedimentary archive recording recurrent giant subduction zone earthquakes and their role in organic carbon export to the deep sea. *Frontiers in Earth Science* 7, 319. <https://doi.org/10.3389/feart.2019.00319>.
- Kobayashi, K., 2004. Origin of the Palau and Yap trench-arc systems. *Geophysical Journal International* 157, 1303–1315. <https://doi.org/10.1111/j.1365-246X.2003.02244.x>.
- Kobayashi, K., Cadet, J.-P., Aubouin, J., Boulègue, J., Dubois, J., von Huene, R., Jolivet, L., Kanazawa, T., Kasahara, J., Koizumi, K., Lallemand, S., Nakamura, Y., Pautot, G., Suyehiro, K., Tani, S., Tokuyama, H., Yamazaki, T., 1987. Normal faulting of the Daiichi-Kashima Seamount in the Japan Trench revealed by the Kaiko I cruise, Leg 3. *Earth and Planetary Science Letters* 83, 257–266. [https://doi.org/10.1016/0012-821X\(87\)90070-7](https://doi.org/10.1016/0012-821X(87)90070-7).
- Kodaira, S., No, T., Nakamura, Y., Fujiwara, T., Kaiho, Y., Miura, S., Takahashi, N., Kaneda, Y., Taira, A., 2012. Coseismic fault rupture at the trench axis during the 2011 Tohoku-oki earthquake. *Nature Geoscience* 5, 646–650. <https://doi.org/10.1038/ngeo1547>.
- Kopp, C., Fruehn, J., Flueh, E.R., Reichert, C., Kukowski, N., Bialas, J., Klaeschen, D., 2000. Structure of the Makran subduction zone from wide-angle and reflection seismic data. *Tectonophysics* 329, 171–191. [https://doi.org/10.1016/S0040-1951\(00\)00195-5](https://doi.org/10.1016/S0040-1951(00)00195-5).
- Krümmel, O., 1907. Handbuch der Ozeanographie. Engelhorn, Stuttgart, 804 p.
- Lay, T., Kanamori, H., Ammon, C.J., Nettles, M., Ward, S.N., Aster, R.C., Beck, S.L., Bilek, S.L., Brudzinski, M.R., Butler, R., DeShon, H.R., Ekström, G., Satake, K., Sipkin, S., 2005. The Great Sumatra-Andaman Earthquake of 26 December 2004. *Science* 308, 1127–1133. <https://doi.org/10.1126/science.1112250>.
- Leat, P.T., Fretwell, P.T., Tate, A.J., Larter, R.D., Martin, T.J., Smellie, J.L., Jokat, W., Bohrmann, G., 2014. Bathymetry and geological setting of the South Sandwich Islands Volcanic Arc (various scales). In: BAS GEOMAP 2 Series, Sheet 6. British Antarctic Survey, Cambridge, UKCambridge, UK. <https://doi.org/10.5285/b8143952-421c-4544-8437-58f33925d30>.
- Leat, P.T., Fretwell, P.T., Tate, A.J., Larter, R.D., Martin, T.J., Smellie, J.L., Jokat, W., Bohrmann, G., 2016. Bathymetry and geological setting of the South Sandwich Islands volcanic arc. *Antarctic Science* 28, 293–303. <https://doi.org/10.1017/S0954102016000043>.
- Lecours, V., Dolan, M.F.J., Micallef, A., Lucieer, V.L., 2016. A review of marine geomorphometry, the quantitative study of the seafloor. *Hydrology and Earth System Sciences* 20, 3207–3244. <https://doi.org/10.5194/hess-20-3207-2016>.
- LOLA Science Team, 2014. Moon LRO LOLA DEM 118 m v1. LOLA Science Team. https://astrogeology.usgs.gov/search/details/Moon/LRO/LOLA/Lunar_LRO_LOLA_Global_LDEM_118m_Mar2014/.
- Luo, M., Glud, R.N., Pan, B., Wenzhöfer, F., Xu, Y., Lin, G., Chen, D., 2018. Benthic carbon mineralization in Hadal Trenches: Insights from in situ determination of benthic oxygen consumption. *Geophysical Research Letters* 45, 2752–2760. <https://doi.org/10.1002/2017GL076232>.
- Magellan Team, 1997. Magellan Global Topography 4641 m v2. PDS GeoScience Node. https://astrogeology.usgs.gov/search/map/Venus/Magellan/RadarProperties/Venus_Magellan_Topography_Global_4641m_v02.
- Matthews, K.J., Maloney, K.T., Zahirovic, S., Williams, S.E., Seton, M., Müller, R.D., 2016. Global plate boundary evolution and kinematics since the late Paleozoic. *Global and Planetary Change* 146, 226–250. <https://doi.org/10.1016/j.gloplacha.2016.10.002>.
- Mayer, L.A., 2006. Frontiers in seafloor mapping and visualization. *Marine Geophysical Researches* 27, 7–17. <https://doi.org/10.1007/s11001-005-0267-x>.
- Mayer, L., Jakobsson, M., Allen, G., Dorschel, B., Falconer, R., Ferrini, V., Lamarche, G., Snaith, H., Weatherall, P., 2018. The Nippon Foundation—GEBCO Seabed 2030 Project: The quest to see the World's oceans completely mapped by 2030. *Geosciences* 8, 63. <https://doi.org/10.3390/geosciences8020063>.
- McHugh, C.M., Seeber, L., Rasbury, T., Strasser, M., Kioka, A., Kanamatsu, T., Ikehara, K., Usami, K., 2020. Isotopic and sedimentary signature of megathrust ruptures along the Japan subduction margin. *Marine Geology* 428, 106283. <https://doi.org/10.1016/j.margeo.2020.106283>.
- Melton, M.A., 1965. The geomorphic and paleoclimatic significance of alluvial deposits in Southern Arizona. *Journal of Geology* 73, 1–38. <https://doi.org/10.1086/627044>.
- Mogi, A., Nishizawa, K., 1980. Breakdown of a Seamount on the Slope of the Japan Trench. *Proceedings of Japan Academy Series B: Physical and Biological Sciences* 56, 257–259. <https://doi.org/10.2183/pjab.56.257>.
- Morra, G., Regenauer-Lieb, K., Giardini, D., 2006. Curvature of oceanic arcs. *Geology* 34, 877. <https://doi.org/10.1130/G22462.1>.
- Müller, R.D., Sdrolias, M., Gaina, C., Roest, W.R., 2008. Age, spreading rates, and spreading asymmetry of the world's ocean crust. *Geochemistry, Geophysics, Geosystems* 9, Q04006. <https://doi.org/10.1029/2007GC001743>.
- Nakamura, Y., Kodaira, S., Miura, S., Regalla, C., Takahashi, N., 2013. High-resolution seismic imaging in the Japan Trench axis area off Miyagi, northeastern Japan. *Geophysical Research Letters* 40, 1713–1718. <https://doi.org/10.1002/grl.50364>.
- Nakanishi, M., Hashimoto, J., 2011. A precise bathymetric map of the world's deepest seafloor, Challenger Deep in the Mariana Trench. *Marine Geophysical Researches* 32, 455–463. <https://doi.org/10.1007/s11001-011-9134-0>.
- Parsons, B., Slater, J.G., 1977. An analysis of the variation of ocean floor bathymetry and heat flow with age. *Journal of Geophysical Research* 82, 803–827. <https://doi.org/10.1029/JB082i005p00803>.
- Pearce, F.D., Rondenay, S., Sachpazi, M., Charalampakis, M., Royden, L.H., 2012. Seismic investigation of the transition from continental to oceanic subduction along the western Hellenic Subduction Zone. *Journal of Geophysical Research: Solid Earth* 117, B07306. <https://doi.org/10.1029/2011JB009023>.
- Peng, G., Bellerby, R., Zhang, F., Sun, X., Li, D., 2020. The ocean's ultimate trashcan: Hadal trenches as major depositories for plastic pollution. *Water Research* 168, 115,121. <https://doi.org/10.1016/j.watres.2019.115121>.
- Piccard, J., Dietz, R.S., 1961. Seven Miles Down: The Story of the Bathyscaphe Trieste. Putnam, 249 p.
- Polonia, A., Torelli, L., Brancolini, G., Loreto, M.-F., 2007. Tectonic accretion versus erosion along the southern Chile trench: Oblique subduction and margin segmentation. *Tectonics* 26, TC3005. <https://doi.org/10.1029/2006TC001983>.
- Reston, T., Fruehn, J., von Huene, R., 2002. The structure and evolution of the western Mediterranean Ridge. *Marine Geology* 186, 83–110. [https://doi.org/10.1016/S0025-3227\(02\)00174-3](https://doi.org/10.1016/S0025-3227(02)00174-3).

- Schwanghart, W., Scherler, D., 2014. Short Communication: TopoToolbox 2—MATLAB-based software for topographic analysis and modeling in Earth surface sciences. *Earth Surface Dynamics* 2, 1–7. <https://doi.org/10.5194/esurf-2-1-2014>.
- Schwestermann, T., Huang, J., Konzett, J., Kioka, A., Wefer, G., Ikehara, K., Moernaut, J., Eglington, T.I., Strasser, M., 2020. Multivariate statistical and multiproxy constraints on earthquake-triggered sediment remobilization processes in the Central Japan Trench. *Geochemistry, Geophysics, Geosystems* 21. <https://doi.org/10.1029/2019GC008861>
- Seton, M., Müller, R.D., Zahirovic, S., Williams, S., Wright, N.M., Cannon, J., Whittaker, J.M., Matthews, K.J., McGirr, R., 2020. A global data set of present-day oceanic crustal age and seafloor spreading parameters. *Geochemistry, Geophysics, Geosystems* 21. <https://doi.org/10.1029/2020GC009214> e2020GC009214.
- Shimanaga, M., Yanagi, K., 2016. The Ryukyu Trench may function as a “depocenter” for anthropogenic marine litter. *Journal of Oceanography* 72, 895–903. <https://doi.org/10.1007/s10872-016-0388-7>.
- Smith, D.E., Zuber, M.T., Frey, H.V., Garvin, J.B., Head, J.W., Muhleman, D.O., Pettengill, G.H., Phillips, R.J., Solomon, S.C., Zwally, H.J., Banerdt, W.B., Duxbury, T.C., Golombek, M.P., Lemoine, F.G., Neumann, G.A., Rowlands, D.D., Aharonson, O., Ford, P.G., Ivanov, A.B., Johnson, C.L., McGovern, P.J., Abshire, J.B., Afzal, R.S., Sun, X., 2001. Mars Orbiter Laser Altimeter: Experiment summary after the first year of global mapping of Mars. *Journal of Geophysical Research, Planets* 106 (23), 689–23722. <https://doi.org/10.1029/2000JE001364>.
- Smith, G., McNeill, L., Henstock, T.J., Bull, J., 2012. The structure and fault activity of the Makran accretionary prism. *Journal of Geophysical Research—Solid Earth* 117, B07407. <https://doi.org/10.1029/2012JB009312>.
- Stein, C.A., Stein, S., 1992. A model for the global variation in oceanic depth and heat flow with lithospheric age. *Nature* 359, 123–129. <https://doi.org/10.1038/359123a0>.
- Stern, R.J., 2002. Subduction zones. *Reviews of Geophysics* 40, 1012. <https://doi.org/10.1029/2001RG000108>.
- Stewart, H.A., Jamieson, A.J., 2018. Habitat heterogeneity of hadal trenches: Considerations and implications for future studies. *Progress in Oceanography* 161, 47–65. <https://doi.org/10.1016/j.pocean.2018.01.007>.
- Stewart, H.A., Jamieson, A.J., 2019. The five deeps: The location and depth of the deepest place in each of the world’s oceans. *Earth-Science Reviews* 197, 102896. <https://doi.org/10.1016/j.earscirev.2019.102896>.
- Strasser, M., Kolling, M., Ferreira, C., Dos, S., Fink, H.G., Fujiwara, T., Henkel, S., Ikehara, K., Kanamatsu, T., Kawamura, K., Kodaira, S., Romer, M., Wefer, G., 2013. A slump in the trench: Tracking the impact of the 2011 Tohoku-Oki earthquake. *Geology* 41, 935–938. <https://doi.org/10.1130/G34477.1>.
- Straume, E.O., Gaina, C., Medvedev, S., Hochmuth, K., Gohl, K., Whittaker, J.M., Abdul Fattah, R., Doornenbal, J.C., Hopper, J.R., 2019. GlobSed: Updated total sediment thickness in the World’s oceans. *Geochemistry, Geophysics, Geosystems* 20, 1756–1772. <https://doi.org/10.1029/2018GC008115>.
- Sykes, T.J.S., 1996. A correction for sediment load upon the ocean floor: Uniform versus varying sediment density estimations—Implications for isostatic correction. *Marine Geology* 133, 35–49. [https://doi.org/10.1016/0025-3227\(96\)00016-3](https://doi.org/10.1016/0025-3227(96)00016-3).
- Taira, K., Yanagimoto, D., Kitagawa, S., 2005. Deep CTD casts in the Challenger Deep, Mariana Trench. *Journal of Oceanography* 61, 447–454. <https://doi.org/10.1007/s10872-005-0053-z>.
- Talwani, M., Sutton, G.H., Worzel, J.L., 1959. A crustal section across the Puerto Rico Trench. *Journal of Geophysical Research* 64, 1545–1555. <https://doi.org/10.1029/JZ064i01p01545>.
- Thomson, C.W., Murray, J., 1895. Report on the Results of the Voyage of H.M.S. Challenger during the Years 1873–76, Narrative, Vol. A(1). HM Stationery Office, London.
- Tovich, A., Gerald, S., 1978. Island arc curvature, velocity of convergence and angle of subduction. *Geophysical Research Letters* 5, 329–332. <https://doi.org/10.1029/GL005i005p00329>.
- Tugend, J., Chamot-Rooke, N., Arsenikos, S., Blanpied, C., Frizon de Lamotte, D., 2019. Geology of the Ionian basin and margins: A key to the east mediterranean geodynamics. *Tectonics* 38, 2668–2702. <https://doi.org/10.1029/2018TC005472>.
- Turcotte, D.L., McAdoo, D.C., Caldwell, J.G., 1978. An elastic-perfectly plastic analysis of the bending of the lithosphere at a trench. *Tectonophysics* 47, 193–205. [https://doi.org/10.1016/0040-1915\(78\)90030-6](https://doi.org/10.1016/0040-1915(78)90030-6).
- Vening Meinesz, F.A., 1932. Gravity expeditions at sea 1923–1930. In: The Expeditions, the Computations and the Results, vol. 1. Nederlandse Commissie voor Geodesie, N.V. Technische Boekhandel en Drukkerij J. Waltman Jr, Delft, 109 pp.
- von Huene, R., Scholl, D.W., 1991. Observations at convergent margins concerning sediment subduction, subduction erosion, and the growth of continental crust. *Reviews of Geophysics* 29, 279–316.
- von Huene, R., Ranero, C.R., Weinrebe, W., Hinz, K., 2000. Quaternary convergent margin tectonics of Costa Rica, segmentation of the Cocos Plate, and Central American volcanism. *Tectonics* 19, 314–334. <https://doi.org/10.1029/1999TC001143>.
- von Huene, R., Miller, J.J., Weinrebe, W., 2012. Subducting plate geology in three great earthquake ruptures of the western Alaska margin, Kodiak to Unimak. *Geosphere* 8, 628–644. <https://doi.org/10.1130/GES00715.1>.
- Watts, A., Koppers, A., Robinson, D., 2010. Seamount subduction and earthquakes. *Oceanography* 23, 166–173. <https://doi.org/10.5670/oceanog.2010.68>.
- Wenzhöfer, F., Oguri, K., Middelboe, M., Turnewitsch, R., Toyofuku, T., Kitazato, H., Glud, R.N., 2016. Benthic carbon mineralization in hadal trenches: Assessment by in situ O₂ microprofile measurements. *Deep-Sea Research Part I: Oceanography Research Paper* 116, 276–286. <https://doi.org/10.1016/j.dsr.2016.08.013>.
- Wessel, P., Smith, W.H.F., 1996. A global, self-consistent, hierarchical, high-resolution shoreline database. *Journal of Geophysical Research: Solid Earth* 101, 8741–8743. <https://doi.org/10.1029/96JB00104>.
- Wessel, P., Luis, J.F., Uieda, L., Scharroo, R., Wobbe, F., Smith, W.H.F., Tian, D., 2019. The generic mapping tools Version 6. *Geochemistry, Geophysics, Geosystems* 20, 5556–5564. <https://doi.org/10.1029/2019GC008515>.
- Wölfel, A.-C., Snaith, H., Amirebrahimi, S., Devey, C.W., Dorschel, B., Ferrini, V., Huvenne, V.A.I., Jakobsson, M., Jencks, J., Johnston, G., Lamarche, G., Mayer, L., Millar, D., Pedersen, T.H., Picard, K., Reitz, A., Schmitt, T., Visbeck, M., Weatherall, P., Wigley, R., 2019. Seafloor mapping—The challenge of a Truly global ocean bathymetry. *Frontiers in Marine Science* 6. <https://doi.org/10.3389/fmars.2019.00283>.